ENERGY LOSS IN CONDENSED MATTER OF H^1 AND He^4

IN THE ENERGY RANGE $4 < E < 30$ keV

ENERGY LOSS IN CONDENSED MATTER OF H^1 AND He^4

IN THE ENERGY RANGE $4 < E < 30$ keV.

by

Arie van Wijngaarden, B.Sc.

A Thesis

Submitted to the Faculty of Graduate Studies

in Partial Fulfilment of the Requirements

for the Degree

Doctor of Philosophy

McMaster University

October 1962

DOCTOR OF PHILOSOPHY (1962)   McMASTER UNIVERSITY
(PHYSICS)   HAMILTON, ONT.

TITLE: Energy Loss in Condensed Matter of H^1 and
       He^4 in the Energy Range $4 < E < 30$ keV.

AUTHOR: Arie van Wijngaarden,

NO. of PAGES: viii, 48 56

NO. of FIGURES:

SCOPE AND CONTENTS:

Measurements are reported of the energy loss
suffered by H^1 and He^4 particles, of 4-30 keV energy,
in passing through thin films of carbon, aluminum-
oxide and VYNS. Only those particles that emerged in
the forward direction were studied. Evidence is
presented for identifying the stopping cross-sections
per atom observed in this way with S_e, the electronic
component of the total stopping cross-section per
atom. It appears that the calculated energy dependence
of $S_e (\propto \sqrt{E})$ is somewhat in error, and that the magni-
tudes of the S_e's for He^4 are systematically too
small by 10-15%.

ACKNOWLEDGEMENTS

C O N T E N T S

Contents - cont'd

LIST OF FIGURES

List of Tables

C H A P T E R   I

Introduction

(1) The Need for Low-Energy Stopping Data

The manner in which heavy particles lose energy in passing through matter is of interest in several branches of physics.

First to take an interest in the subject were nuclear physicists who wished to employ range-energy curves to determine charged-particle energies. From this interest has grown an extensive body of literature which has recently been summarized by Whaling (1958) for the energy range $0 < E < 10$ MeV. Most of the data presented by Whaling relate to protons, deuterons and alpha-particles. As it happens, charged particle energy determinations are now made with much greater precision using magnetic and electrostatic analysers, with the result that the original interest in range-energy relationships has been replaced by a need to correct observed energies for the relatively small energies lost in the source. Thus, in Whaling's article, the old range-energy curves have been superseded by curves presenting the differential energy loss $(\frac{dE}{dx})$ as a function of energy. In the energy region below 50 keV the tabulated data come almost entirely from two experiments (Phillips, 1953; Reynolds, Dunbar, Wenzel and Whaling, 1953), in both of which protons lost energy to gases confined in gas cells. In Phillips' experiment the energy

range was $10 < E < 80$ keV while in that of Reynolds et al
it was $30 < E < 600$ keV. The lack of agreement in the
region of overlap has prompted Whaling to remark that
"Further experiments in this energy region would be
desirable".

A relatively new area of application of energy loss
data is the study of nuclear reactions by the observation
of recoiling nuclei. In many cases where more than one
particle is emitted in a nuclear reaction, the only
practicable way to follow the course of events is to
observe the recoil of the nucleus. The importance of this
type of approach has recently been stressed by Harvey
(1960), who deplores the lack of energy-loss data for low-
speed, heavy particles. Normally, of course, the "heavy"
particle is heavier than a proton or alpha particle, but
whatever knowledge is gained concerning lighter particles
will presumably aid in rationalizing and predicting the
behaviour of heavy ones.

The study of radiation damage to solids represents a
third important area in which existing energy-loss informa-
tion is utilized, and additional information is desired
(Seitz and Koehler, 1956; Billington and Crawford, 1961).

Energy loss data are also important for the inter-
pretation of secondary electron emission and luminescence
under low speed ion bombardment. By using some of the
experimental results presented in this thesis, the author
has recently made progress, as yet unpublished, in inter-

preting these phenomena.

Finally, further experimental work is called for in order to subject to trial certain recent calculations of the differential energy losses suffered by heavy, low-speed particles. This matter has been the subject of a good deal of study (Bohr, (1948); Lindhard and Scharff (1953); Lindhard (1954); Nielsen (1956); Seitz and Koehler (1956); Holmes and Leibfried (1960); Lindhard and Scharff (1961); the present author (see section I,2,d), and others) and it has now reached the point where a comparison with experiment in the energy range $0 < E < 50$ keV is highly desirable. The experiments to be described go a long way towards providing this comparison for H^1 and He^4. Other experiments which are currently underway in this laboratory (Ormrod and Duckworth (1962) utilize heavier particles, and should help further to clarify the picture.

(2) Theory

    (a) Introduction

We shall outline briefly, in general following the recent summary by Lindhard and Scharff (1961), the mechanism by which low-speed, heavy ions are thought to lose energy.

For particles with velocity $v \lesssim v_0$ (where $v_0 = \dfrac{2\pi e^2}{h}$ is the velocity of the electron in the first Bohr orbit in hydrogen), energy is lost both to electrons in the stopping medium and to recoiling atoms, with the latter

effect becoming more important as the velocity of the particle decreases. Thus the total stopping cross-section per atom of stopping medium may be written as

$$S = S_e + S_n \qquad (1)$$

where the subscripts e and n refer to the electronic and atomic (or nuclear) components, respectively.

The differential energy loss, dE/dx, is related to the stopping cross-section per atom through the relationship

$$\frac{dE}{dx} = - NS \qquad (2)$$

where N is the number of stopping atoms per unit volume. The quantity -dE/dx, the negative of the differential energy loss, is known as the stopping power of the medium for the particles under study.

(b) Loss in Energy to Electrons

S_e may be calculated by assuming that the particle moves through an electron gas of constant density .. a model first introduced by Fermi and Teller (1947) to study the slowing down of negative muons.[*] The actual expression deduced by Lindhard and Scharff is valid only for particle velocities that are small compared to $v_o Z_1^{2/3}$ (where Z_1 is the atomic number of the particle) and has the value

$$S_e = \xi_e \left[8\pi e^2 a_o \right] \left[\frac{Z_1 Z_2}{\left(Z_1^{2/3} + Z_2^{2/3} \right)^{3/2}} \right] \left[\frac{v}{v_o} \right] \qquad (3)$$

Here Z_2 is the atomic number of the stopping atom, a_o is

[*] See Appendix

the Bohr radius and ξ_e is of the order $1-2$, possibly having the value $Z_1^{1/6}$. In fact, the value used by Powers and Whaling (1962) is

$$\xi_e = Z_1^{1/6}$$

With this value equation (3) can be written in the form

$$S_e = Z_1^{1/6} \left[8\pi e^2 a_0 \right] \left[\frac{Z_1 Z_2}{(Z_1^{2/3} + Z_2^{2/3})^{3/2}} \right] \sqrt{\frac{E}{E_{v_0}}} \qquad (4)$$

where E_{v_0} is the kinetic energy of the projectile when its speed equals

$$v_0 \simeq 2.2 \times 10^8 \, \text{cm sec}^{-1}$$

The values of E_{v_0} for H^1 and He^4 are 25 keV and 100 keV, respectively. For $v \gtrsim v_0 Z_1^{2/3}$, the expression no longer holds and S_e gradually assumes a $(\ln E)/E$ dependence (Bloch 1933).

Thus the preceding equation can only be used at energies below about 250 keV for the slowing down of atomic helium and at energies below approximately 25 keV for atomic hydrogen. However, in the experiments to be described, we shall later apply the S_e formula to the stopping of atomic hydrogen and of atomic helium in the energy interval $0 < E < 30$ keV. In this energy interval, equation (3) holds for the slowing down of atomic helium but does not hold for the stopping of atomic hydrogen in the energy interval $25 < E < 30$ keV.

Thus, we shall not be able to compare theory and experiment rigorously for atomic hydrogen in the energy

range studied. However, perfect agreement with theory
cannot be anticipated anyway, since the formulas for
S_e are merely approximations (the $E^{1/2}$ dependence is
only approximate and ξ_e is quite uncertain) to the
cross-section for loss in energy to electrons.

(c) Loss in Energy in Atomic Recoils

The form of S_n was first studied by Bohr (1948) who
assumed that atomic collisions occur in a potential

$$P(r) = e^2 \frac{Z_1 Z_2}{r} e^{-r/a} \qquad (5)$$

where r is the distance between the nuclei of the colliding
particles and a is the so-called screening parameter.
The value of the screening parameter used by Lindhard
and Scharff is

$$a = \frac{0.8853\ a_o}{\sqrt{Z_1^{2/3} + Z_2^{2/3}}} \qquad (6)$$

In this type of potential the distance of closest approach,
b', in a head-on collision is given by

$$\frac{b}{a} = \frac{b'}{a} e^{(b'/a)} \qquad (7)$$

where b, the distance of closest approach if the colliding
particles were stripped of their planetary electrons, has
the value

$$b = 2 Z_1 Z_2 e^2 \left[\frac{M_1 + M_2}{M_1 M_2 v^2} \right] \qquad (8)$$

where M_1 is the mass of the projectile of velocity, v, and

M_2 is the mass of the target particle. From now on we shall denote the quotient b'/a by

$$s = \frac{b'}{a}$$

For the purpose of showing the behavior of s with energy we have tabulated in Table I some values of s corresponding to collisions of a number of different atomic projectiles with a carbon atom, initially at rest.

Table 1

E	$s = b'/a$			
keV	H^1	He^4	N^{14}	A^{40}
1	0.28	0.56	1.5	2.8
5	0.073	0.17	0.7	1.7
10	0.037	0.09	0.4	1.3
20	0.018	0.05	0.3	0.9
60			0.1	0.5

Bohr expands equation (5) and finds that the assumed potential may be approximated by

$$P_n(r) = Z_1 Z_2 e^2 a^{n-1} \left[\frac{n-1}{2.71} \right]^{n-1} r^{-n} \qquad (9)$$

where $n = 1 + r/a$.

The effect of different values of r on the field can easily be seen from Equation (9); for instance, if $r \ll a$ the potential is with high approximation coulombic. It is

thus of importance to investigate in which part of the field the scattering effectively takes place. A measure of this is the value of the parameter s. For instance, at relatively high energies, $s \ll 1$, so that most of the scattering effectively takes place at a distance, r, which is small compared to a . Under these conditions, n is only slightly larger than unity and the scattering, therefore, is predominantly of the Rutherford type (that is, in a coulombic potential). In this energy range, Bohr finds $Sn_{s<1}$, the stopping cross-section for loss in energy to atomic recoils, to be given approximately by

$$Sn_{s<1} \simeq 2\pi \frac{M_1}{M_2} \quad \frac{e^4 Z_1^2 Z_2^2}{E} \quad \ln\left[\frac{2a}{Z_1 Z_2 e^2} \quad \frac{M_2 E}{M_1 + M_2} \right] \quad (10)$$

For lower energies of the impinging particle, a increases in value, and the scattering takes place to an increasing extent in the screened part of the field. Thus, in the energy range where $s \sim 1$ the scattering takes place entirely in the screened part of the field, $(r \sim a)$, which falls off more rapidly than does the coulomb field. In this energy region, the n value is approximately

$$n \simeq 2$$

For the corresponding inverse square potential $(P(r) \propto \frac{1}{r^2})$ Lindhard and scharff (1961) find, in good agreement with Nielsen (1956) that

$$Sn_{s \sim 1} = 1.13\left[\frac{\pi^2 e^2}{2.71} \quad a \, Z_1 Z_2 \quad \frac{M_1}{M_1 + M_2} \right] \quad (11)$$

represents a first order approximation to the actual cross-section for loss in energy in atomic recoils.

Approximations for S_n for still lower energies are given by the following formula:

$$(S_n)_n = (\frac{1}{n-1}) \pi^{3-2/n} \left[\frac{n \, I_n}{2}\right]^{2/n} e^{4/n} \left[\frac{n-1}{2.71}\right]^{2-2/n} \left[a^{2-2/n} (Z_1 Z_2)^{2/n} \left(\frac{M_1}{M_1 + M_2}\right) \left(\frac{M_2 E}{M_1 + M_2}\right)^{1-2/n} \right] \quad (12)$$

where

$$I_n = \int_{-\infty}^{+\infty} \frac{dt}{(1 + t^2)^{\frac{n+2}{n}}}$$

Equation (12), which will be derived in the next section, has been deduced by the author and is valid for any value of $n \gtrsim 2$.

When $n = 2$ Equation (12) reduces to

$$S_{n_{s \sim 1}} = 1.57 \left[\frac{\pi^2 e^2}{2.71} \, a \, Z_1 Z_2 \, \frac{M_1}{M_1 + M_2}\right]$$

which is in fair agreement with Equation (11).

Lindhard and Scharff state in their 1961 publication, without presenting a derivation for the following formula or Equation (11), that in a power potential of the form

$$P(r) \propto \frac{Z_1 Z_2}{r^n} \, a^{n-1} \quad \text{(See Equation (9)}$$

the energy loss cross-section behaves as

$$(S_n)_n \propto a^{2-2/n} (Z_1 Z_2)^{2/n} \left[\frac{M_1}{M_1 + M_2}\right] \left[\frac{M_2 E}{M_1 + M_2}\right]^{1-2/n}$$

in agreement with our result, Equation (12).

To summarize: we have Equation (10) representing a first-order approximation to S_n at high energies ($s \ll 1$). At lower energies, where $s \sim 1$, S_n can be approximated by Equation (11) or by Equation (12) with n = 2. At still lower energies ($s \gtrsim 1$), the approximation is given by Equation (12) with $n \sim 3$; et cetera.

Physically we require that in a plot of S_n versus energy, the successive approximations smoothly join each other. From this, and from the energy dependence of the various approximations, it is seen that S_n qualitatively has the form as shown in Figure 1.

In the experiments to be described on the slowing down of atomic hydrogen and helium in the energy range $5 < E < 30$ keV, the parameter s was always less than 0.5 and usually much less than 0.5 (see Table 1). Equation (10) is, therefore, the relevant expression to be used in computing S_n for these atomic particles. On the other hand, the slowing down of atomic argon in the same energy region (see Table 1) should be described by Equation (12) with $n \gtrsim 2$.

(d) Loss in Energy to Atomic Recoils in a Lower Potential.

In this section, we shall present a derivation of Equation (12)
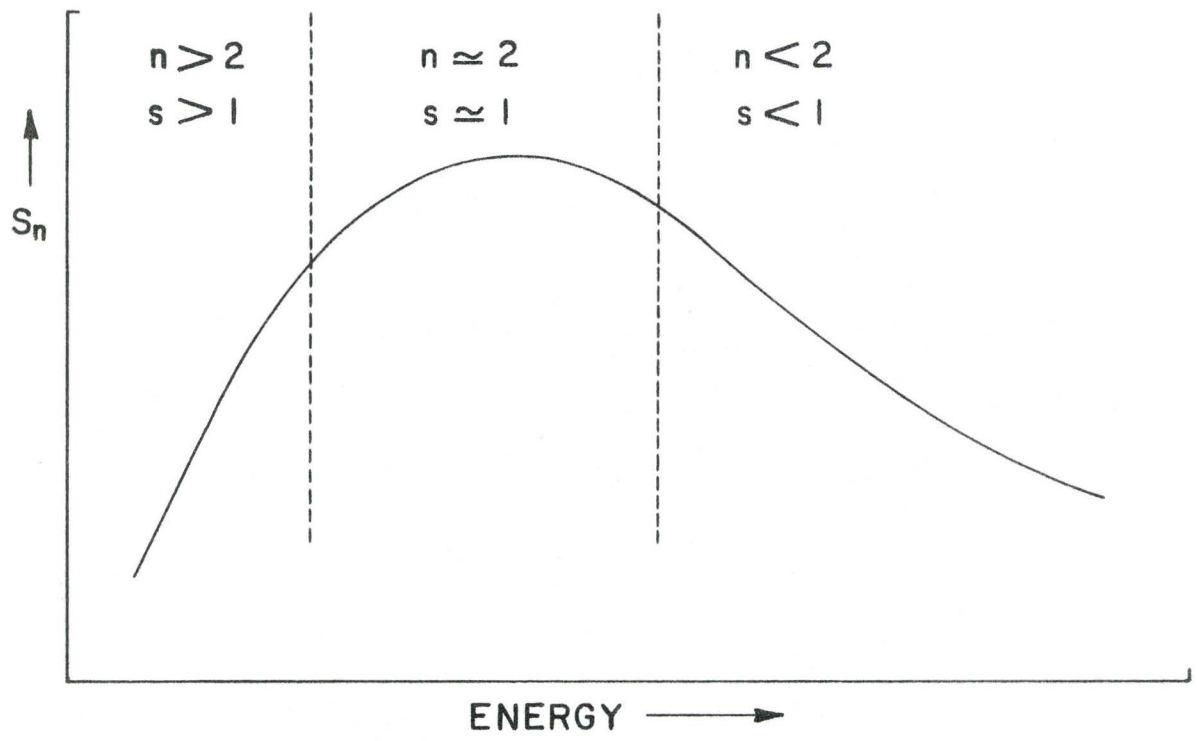
Figure 1 - A Qualitative Presentation of the
Energy Dependence of the Nuclear Component, S_n,
of Total Stopping Cross Section per Atom
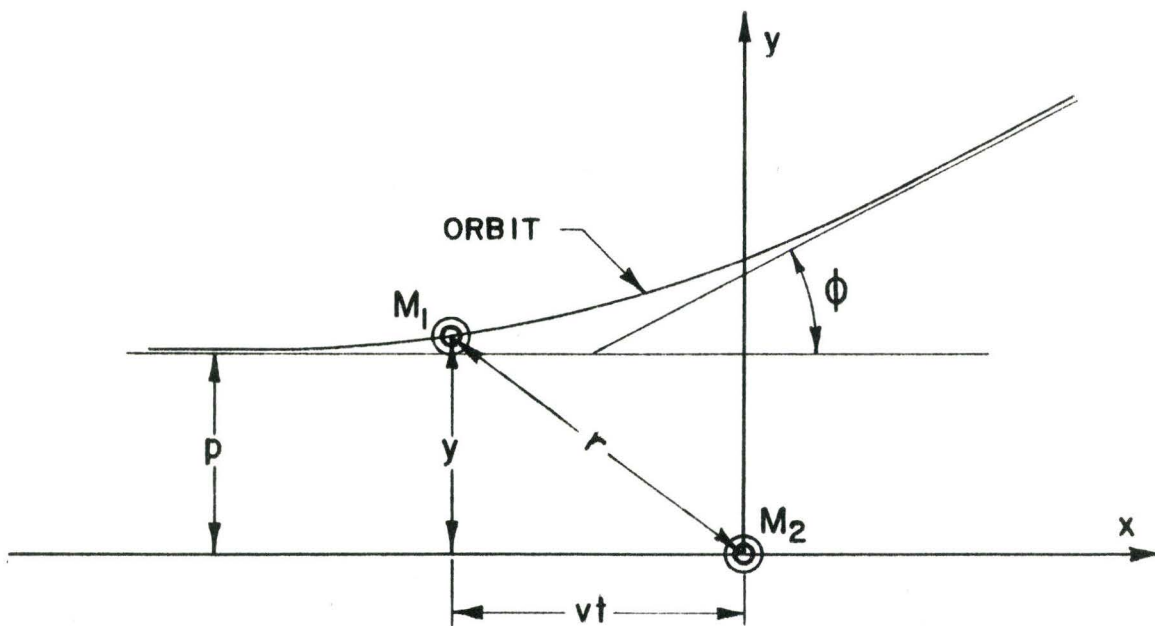
Figure 2 - The Scattering of a Projectile, Mass M1,
by an Arbitrary Central Force, Centered at the
Target Particle of Mass M2.

In a collision between a projectile of mass M_1
and a target particle of mass M_2 the projectile will
describe an orbit and suffer a net deflection angle ϕ.
This has been illustrated in Figure 2 where p, the
impact parameter, would be the distance of closest
approach if no forces were acting between the colliding
particles.

Actually, the struck particle will also describe
an orbit. For clarity in the figure, however, we have
shown the target particle as infinitely heavy, even
although we shall take its motion into account.

The differential cross-section, $d\sigma$, for collisions
between impact parameters p and $p+dp$ is

$$d\sigma = 2\pi p \, dp \qquad\qquad (13)$$

This equation implies that distant collisions (large p)
occur more frequently than the more violent collisions
(small p) in which the particles involved are deflected
through large angles. Because of this the loss in
energy will be mainly determined by the frequent small
angle deflections rather than by the occasional large
angle events.

With this in mind, we shall deduce energy-loss
expressions which are very nearly exact in the limit of
small angle scattering (within the limitations of the
assumptions involved), but which are only crude approxima-
tions to the large angle case. Roughly, however, all
angular scattering events will be taken into account.

In distant collisions, the incident particle is

but little deflected. If all the momentum of the pro-
jectile is originally in the X direction, the struck
particle will be set in motion with momentum M_y in a
direction that is practically perpendicular to the
direction of the incident particle. By Newton's second
law

$$M_y = \int_{-\infty}^{+\infty} F(y)\,dt \qquad (14)$$

where

$$F(y) = \frac{y}{r} F(r) \qquad (15)$$

and r is the distance between the colliding particles.
For distant collisions, see Figure 2.

$$r \simeq (p^2 + v^2 t^2)^{1/2} \qquad (16)$$

where v is the velocity of the projectile.

During the collision the incident particle also
receives a y-component of momentum, which is just equal,
but opposite, to M_y. Hence, the relative deflection
angle, α, of the incident particle equals

$$\alpha \simeq \frac{M_y}{M} \qquad (17)$$

where M, which remains practically unchanged in a distant
collision, is the original momentum (of the projectile)
in relative co-ordinates and is given by

$$M = \frac{M_1 M_2}{M_1 + M_2} v \qquad (18)$$

Evidently the relationship between the actual deflection
angle, ϕ, of the moving particle and the relative deflec-
tion angle is given by

$$\tan \phi = \frac{M_2 \sin \alpha}{M_1 + M_2 \cos \alpha} \tag{19}$$

By means of Equations (14), (15), (16) and (17), we find that

$$\alpha \simeq \int_{-\infty}^{+\infty} \frac{p \, F\left(\sqrt{p^2 + v^2 t^2}\right)}{M \sqrt{p^2 + v^2 t^2}} \, dt \tag{20}$$

By introducing the new variable

$$Z = vt/p$$

we see (see Equation (16) that

$$r = p\sqrt{1 + Z^2} \tag{21}$$

Upon substitution of Equations (21) and (18) into (20) it follows that

$$\alpha \simeq \left(\frac{M_1 + M_2}{M_2}\right) \frac{p}{2E} \int_{-\infty}^{+\infty} \frac{F(p\sqrt{1 + Z^2})}{\sqrt{1 + Z^2}} \, dZ \tag{22}$$

where $\quad E = \frac{1}{2} M_1 v^2$

We shall now apply our equations to a field of force defined by the potential

$$F_n = \frac{k_n}{r^n} \tag{23}$$

which, with

$$k_n = Z_1 Z_2 e^2 a^{n-1} \left(\frac{n-1}{2.71}\right)^{n-1} \tag{24}$$

is the Bohr potential, Equation (9), for atomic collisions. Hence, the force, $F(r)$, equals

$$F(r) = - \frac{n \, k_n}{r^{n+1}} \tag{25}$$

From Equations (25), (21) and (20) we find

$$\alpha \simeq -\left(\frac{M_1 + M_2}{M_2}\right) n \; \frac{p^{-n} k_n I_n}{2E} \qquad (26)$$

where

$$I_n = \int_{-\infty}^{+\infty} \frac{d \, Z}{\left(1 + z^2\right)^{\frac{n+2}{n}}}$$

Evidently

$$I_2 = \frac{\pi}{2}$$

The differential cross-section, $d\sigma$, can be found now by substitution of Equation (26) into (13). This yields

$$d\sigma = -\frac{2\pi}{n}\left[\left(\frac{M_1 + M_2}{M_2}\right) \frac{n \; k_n I_n}{2E}\right]^{2/n} \frac{1}{\alpha^{\frac{2+n}{n}}} \; d\alpha \qquad (27)$$

or

$$d\sigma = -\frac{1}{n}\left[\left(\frac{M_1 + M_2}{M_2}\right) \frac{n \; k_n I_n}{2E}\right]^{2/n} \frac{1}{\alpha^{\frac{2+2n}{n}}} \; d\omega$$

where for small angles the solid angle, $d\omega$, equals

$$d\omega = 2\pi\alpha d\alpha$$

The energy, T, transferred to particle M_2 during the collision can easily be shown to be

$$T = \frac{2 M_1^2 M_2 \; v^2 \; \sin^2 \frac{\alpha}{2}}{\left(M_1 + M_2\right)^2}$$

which for small angles reduces to

$$T \simeq \frac{M_1 M_2}{\left(M_1 + M_2\right)^2} \; E \; \alpha^2 \qquad (28)$$

The average cross-section for energy loss, taking all angular deflections into account, is given by

$$S_n = \int_0^\pi T \, d\sigma \tag{29}$$

On substitution of Equations (27) and (28) into the above, it follows that

$$(S_n)_n = \left(\frac{1}{n-1}\right) \pi^{3-2/n} \left(\frac{n \, k_n I_n}{2}\right)^{2/n} \left(\frac{M_1}{M_1+M_2}\right) \left(\frac{M_2 E}{M_1+M_2}\right)^{1-2/n} \tag{30}$$

Equation (12) can now be deduced by inserting the value for k_n (Equation 24) into the preceding formula.

C H A P T E R   II

Apparatus

(1) Principal Apparatus

A schematic diagram of the apparatus is shown in Figure 3. The principal parts of the apparatus are (1) a source of ions; (2) a ten-inch sector type mass spectrometer, which serves as the ion-analyser; (3) a thin film, in which the ions lose energy; (4) an electrostatic analyser for determining the energy of the ions that emerge from the film in the forward direction, and (5) an electron multiplier for detecting the ions that are transmitted by the electrostatic analyser. The output of the electron multiplier is connected to an amplifier feeding a scalar. Connected to the scalar is a rate-meter from which the number of ions emerging from the electrostatic analyser per unit time interval is read directly.

The film can be removed from the path of the ions (thereby permitting the initial energy of the ions to be determined), and can be rotated through an angle Θ, (thereby increasing its effective thickness to the value $t' = t/\cos\Theta$). The acceptance angle of the electrostatic analyser is 1.2^{o}, and the analyser itself is used as a direction focusing device.

The whole assembly is evacuated, to a pressure of a few times 10^{-6} mm of Hg, by standard vacuum techniques,
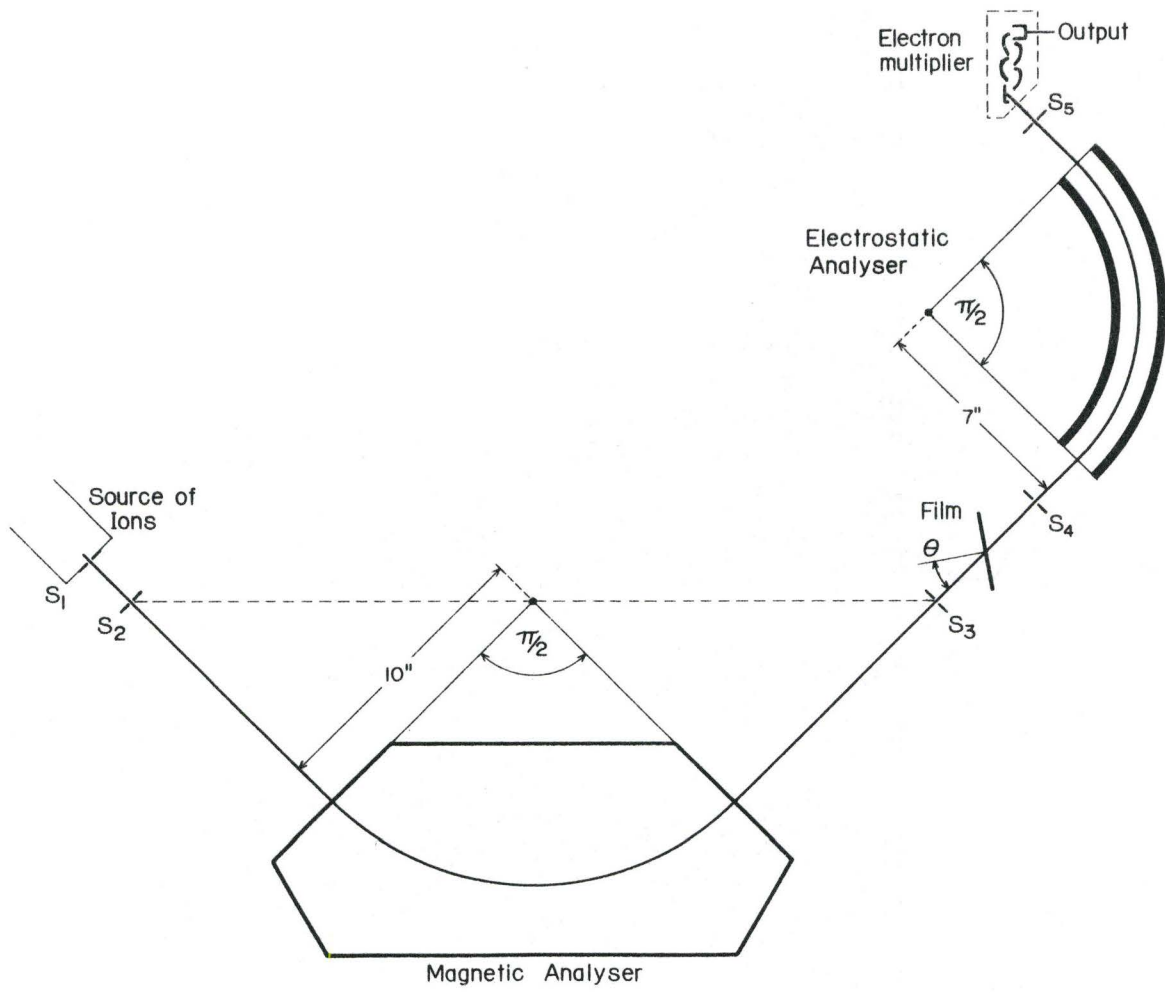
FIGURE 3 - Schematic Diagram of the Apparatus.
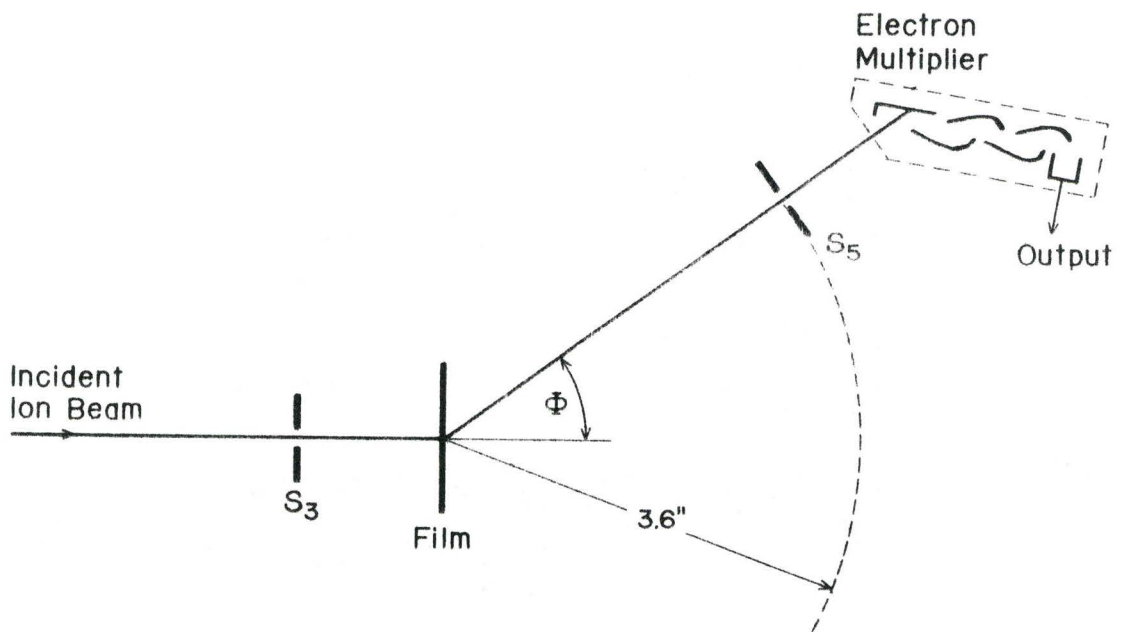
FIGURE 4 - Modification for Studying Angular Distribution of Transmitted
Particles.

utilizing oil diffusion pumps and a rotary mechanical pump.

(2) Apparatus for the Angular Distribution of the Transmitted Beam

For certain experiments, the electrostatic analyser was removed and the electron multiplier was attached to the rest of the apparatus through a bellows system. A schematic diagram of this part of the apparatus is shown in Figure 4. In this way the angular distribution (but not the energy) of the ions emerging from the film could be studied.

(3) Mounting of the Thin Films

Preliminary experiments indicated that the VYNS and Al_2O_3 foils, when subjected to ion bombardment became positively charged to potentials of the order of 1000 volts. This charging-up effect, however, could be eliminated by mounting the thin film on a metal holder, in such a manner that part of the impinging ion beam bombarded the holder. Since the number of secondary electrons emitted by a metal per incident ion, of energies above a few keV, is generally larger than unity (this was investigated in detail in some unpublished work) the charge on the film was neutralized by these secondaries. In this thesis only results that were obtained with uncharged films will be presented.

(4) Thin Films

The thin films are of three types: VYNS,
aluminum oxide (Al_2O_3) and carbon. The VYNS films
were prepared in a manner suggested by the work of
Revell et al (1955) and although their actual thicknesses
are not known, thin specimens could easily be prepared
and were useful in establishing or confirming certain
functional relationships. The aluminum oxide films were
made by anodic oxidation of sheet aluminum. With a
solution of ammonium citrate as the anodizing bath, the
thickness of the oxide layer was taken to be 13.7 $\overset{o}{A}$ per
volt. The aluminum substrate was then removed by hydro-
chloric acid. The anodic oxidation of aluminum in
ammonium citrate has recently been studied by Davies
(1960). The carbon films were produced by evaporation
onto a clean glass slide. When the slide was dipped in
water, the film floated free and could be picked up on
the film holder. Because these carbon films are very
fragile, they required a support which consisted of a
finely-meshed metal screen. Owing to this metal backing,
the unit when rotated through an appreciably large angle
became almost opaque to an ion beam. Consequently,
experiments in which Θ (see Figure 3) was varied were not
carried out with a carbon film, but were only performed
with VYNS and aluminum-oxide foils.

The values of N for the aluminum oxide and carbon
are taken to be 1.03×10^{23} atoms/cm^3 and 1.13×10^{23}
atoms/cm^3, respectively.

C H A P T E R   I I I

Experimental Results on Energy Loss

(1) Observations of the Energy Loss of H^1 in Thin Films

(a) Energy Loss of H^1 in Aluminum Oxide and VYNS.

A typical set of experimental results is shown in Figure 5. These data were obtained with protons of energy E_0 (= 17.49 keV) incident upon a 205 Å film of aluminum oxide. The sharp peak at E_0 was observed by removing the film and reducing the ion current to a value much lower than was needed when the film was in position. The finite resolution of the electrostatic analyser accounts for practically the entire width of this peak. The $\Theta = 2.5^0$ curve shows the energy distribution in the detected ion beam with the film in position and 2.5^0 (nominally 0^0) from being normal to the incident beam. The $\Theta = 42.5^0$, $\Theta = 57.5^0$ and $\Theta = 67.5^0$ curves were obtained by rotating the film to secure successively larger effective film thicknesses ($t' = t/\cos\Theta$)

The difference, ΔE_0, between the initial energy, E_0, and the maximum of the transmitted distributions is the most probable value of the energy lost by the particle in passing through that particular thickness of film. ΔE_0, of course, increases with film thickness. It is assumed that the average energy, $\bar{E}$, of the particle whilst traversing the film is $E_0 - \dfrac{\Delta E_0}{2}$.
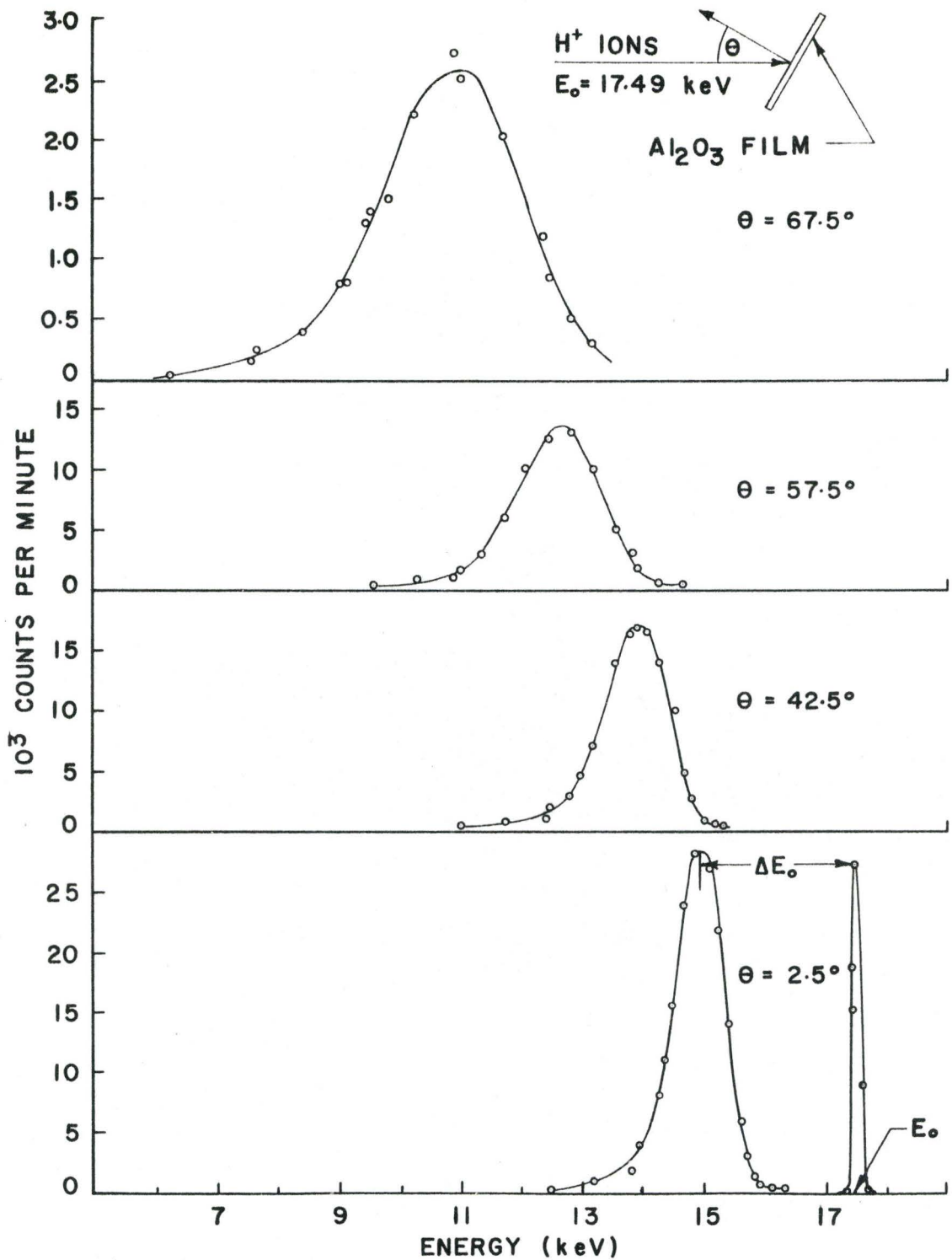
Figure 5 - Energy Distribution Amongst H[1] Particles
after Traversing Al_2O_3 Films of Various Thicknesses

Curves similar to those of Figure 5 were obtained for several different incident energies. From these, values of ΔE_0 and $\bar{E}$ were obtained which form the basis for the $\ln \Delta E_0$-versus-$\ln \bar{E}$ plot shown in Figure 6.

We proceed now to obtain a stopping cross-section-versus-energy curve from Figure 6.

As mentioned earlier, the stopping power of a material for a given particle is defined as $-\dfrac{dE'}{dx}$, where dE is an infinitesimal small energy loss suffered by the particle in travelling an infinitesimal distance, dx, in the stopping medium. How closely does the expression $-\dfrac{\Delta E_0}{t'}$ formed from our observables correspond to $-\dfrac{dE}{dx}$? We answer this question by referring to Table II, in which for several values of $\bar{E}$, the computed values of $\dfrac{\Delta E_0}{t'}$ are tabulated for each of four film thicknesses. The necessary values of ΔE_0 have been read off from the experimental curves plotted in Figure 6.

Table II

$\bar{E}$ (keV)	$\Delta E_0/t'$ (eV/Å)			
	$t' = 205\text{Å}$ ($\Theta = 2.5^{\circ}$)	$t' = 278\text{Å}$ ($\Theta = 42.5^{\circ}$)	$t' = 383\text{Å}$ ($\Theta = 57.5^{\circ}$)	$t' = 536\text{Å}$ ($\Theta = 67.5^{\circ}$)
30	16.3	17.1	16.7	17.2
20	13.8	14.4	14.2	14.4
15	12.1	12.7	12.5	12.6
10	10.3	10.6	10.7	
5	7.4	7.5		
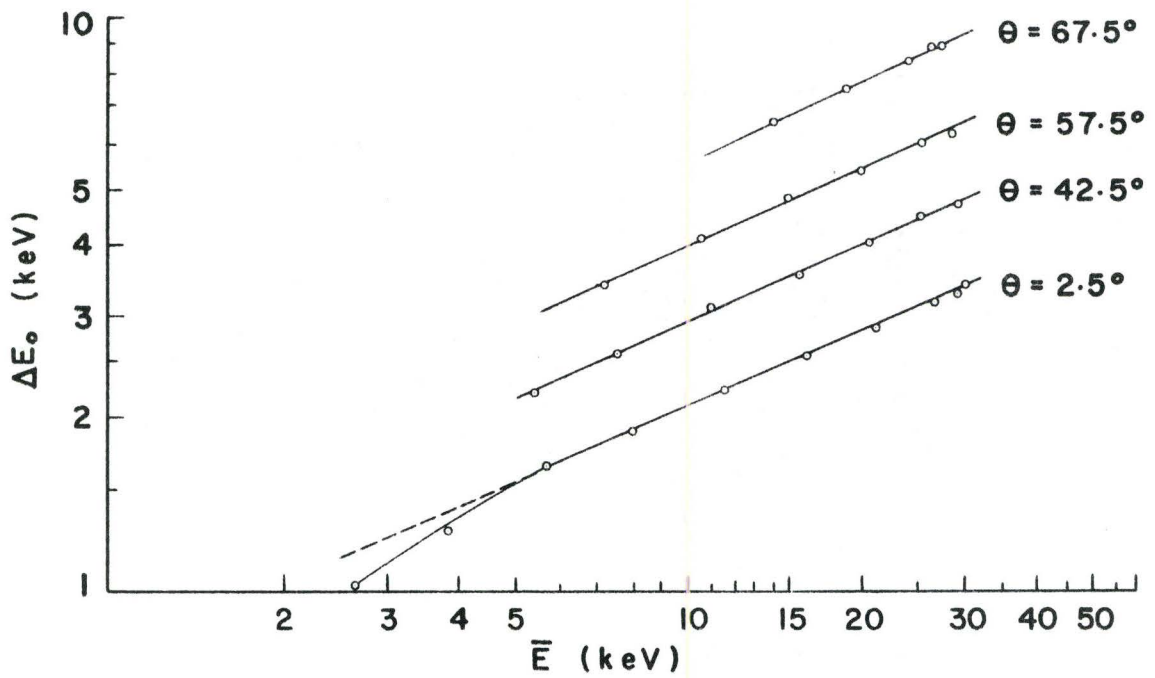
Figure 6 - Log - Log Plot Showing, for Various
Film Thicknesses, the Most Probable Energy Loss
as a Function of Average Particle Energy. The
Curves Relate to H^1 Moving in Al_2O_3

It is evident from Table II that for a given average energy, $\bar{E}$, the value $\frac{\Delta\bar{E}_0}{t'}$ does not change much, if at all, as the thickness of the film changes. The constancy of the value $\frac{\Delta E_0}{t'}$ as t' decreases from $536\overset{\circ}{A}$ to $205\overset{\circ}{A}$ strongly suggests that it is essentially the same in the range $205\overset{\circ}{A} > t' > 0$ as well. This result, indicating that our $\frac{\overline{\Delta E_0}}{t'}$ values actually correspond to stopping powers at energies $E = \bar{E}$ was confirmed by using VYNS films, as we observe from Table III.

<p style="text-align:center">Table III</p>

$\bar{E}$	$\Delta E_0/t'$ (arbritrary units)			
keV	$\theta = 4°$	$\theta = 54°$	$\theta = 69°$	$\theta = 76.5°$
30	17.5	17.4	17.9	17.7
25	16.2	16.1	16.8	16.8
20	14.6	14.6	15.4	15.2
15	13.0	12.9	13.6	13.4
10	10.6	10.8	11.1	10.8
6	8.4	8.4	8.6	8.2
4	6.8	6.8	6.9	6.5

This table, which is similar to Table II, has been compiled from the observed energy loss measurements of a beam of H^1 in passing through a VYNS film. The confirmation is especially valuable at lower energies since the relative thinness of the VYNS films made it possible for all four values of t' to be utilized even with average energies as low as $\bar{E} = 5$ keV.

We have, therefore, obtained $\frac{dE}{dx}$ values from the observed $\frac{\Delta E_o}{t'}$ values (utilizing the $\Theta = 2.5^o$ results as the most reliable, inasmuch as an error in the determination of the angle is least critical for these), and used Equation (2) to calculate corresponding values of the stopping cross-section per atom, S_o, as observed in our experiment. We shall later see that S_o is practically identical to S_e, the electronic component of the total stopping cross-section per atom, but for the time being shall refer to it as the "observed" stopping cross-section per atom. In Figure 7, S_o is plotted against E.

We might also have plotted $\ln S_o$ against $\ln E$, but the reader will realize that such a curve would have had the same shape as the $\Theta = 2.5^o$ curve in Figure 6. It will be noted that, in the energy range $6 < \bar{E} < 30$ keV, this latter curve is closely linear. Hence, we conclude that the $\ln S_o$- versus- $\ln E$ is also linear in this energy range. Furthermore, by using the known values of t' ($205 \overset{o}{A}$) and N (1.03×10^{23} atoms/cm^3), we find the following empirical relationship:

$$S_o = 4.3 \times 10^{-15} \ E^{0.45} \ \text{eV-cm}^2 \qquad (31)$$

in the energy range 6 keV $< E < 30$ keV.

Using VYNS films, it was demonstrated that an empirical relationship similar to Equation (31) exists for this material as well. But since the film thicknesses were not known, it was not possible to calculate the
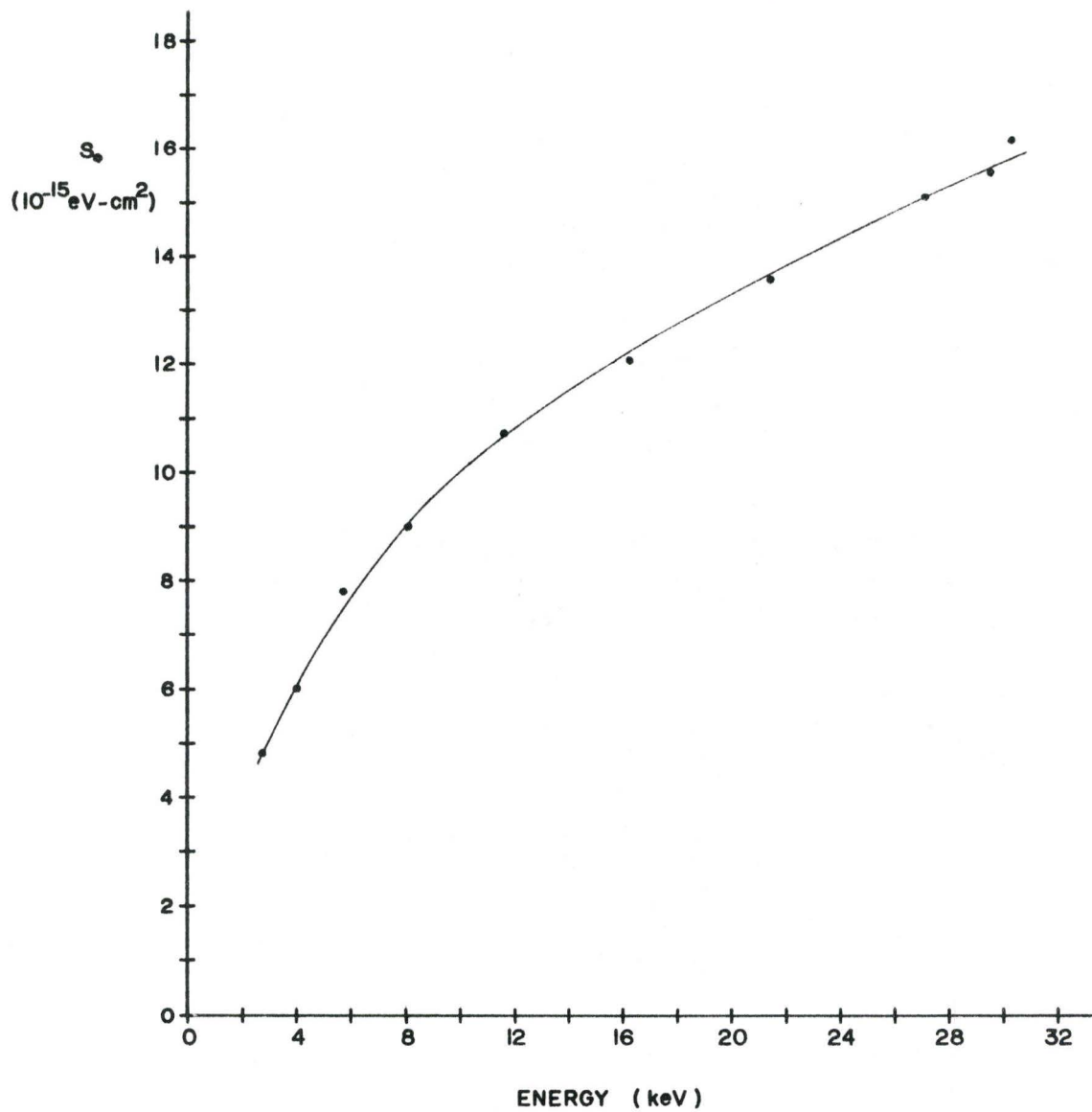
Figure 7 - Plot of Observed Stopping Cross Section per Atom as Function of Energy, for Case of H^1 Moving in Al_2O_3

value of the proportionality constant. The value of
the exponent, however, was precisely the same, namely,
0.45.

(b) <u>Energy Loss of H^1 in Carbon.</u>

Experiments similar to those described for
aluminum oxide and VYNS were also done with a carbon
film. This film was always kept normal to the incident
ion beam and experiments in which θ was varied were not
carried out with it. The energy distribution curves,
which were obtained were similar to those shown previously
for aluminum oxide, and will be further discussed in
Chapter I V

The thickness of the film was not measured directly
but was estimated in the following manner. Whaling (1958)
gives a   ln S - versus - ln E curve for H^1 moving in
carbon with energies greater than 100 keV. This curve
is reproduced in Figure 8 as a solid smooth curve. Our
$\frac{dE}{dx}$ (that is, $\Delta E_0/_t$') - versus - E (that is, $\bar{E}$) curve, which
extends from 4 keV to 30 keV, and which is marked in
Figure 8 with circles, was matched to Whaling's curve by
assuming a value for the thickness of the film which
allowed the two curves to be connected, as shown in
Figure 8, by a dotted line. Although there is consider-
able latitude in this matching, it appears that the film
was about 250Å units thick. Using this value, we have
plotted for H^1 in carbon the stopping cross-section per
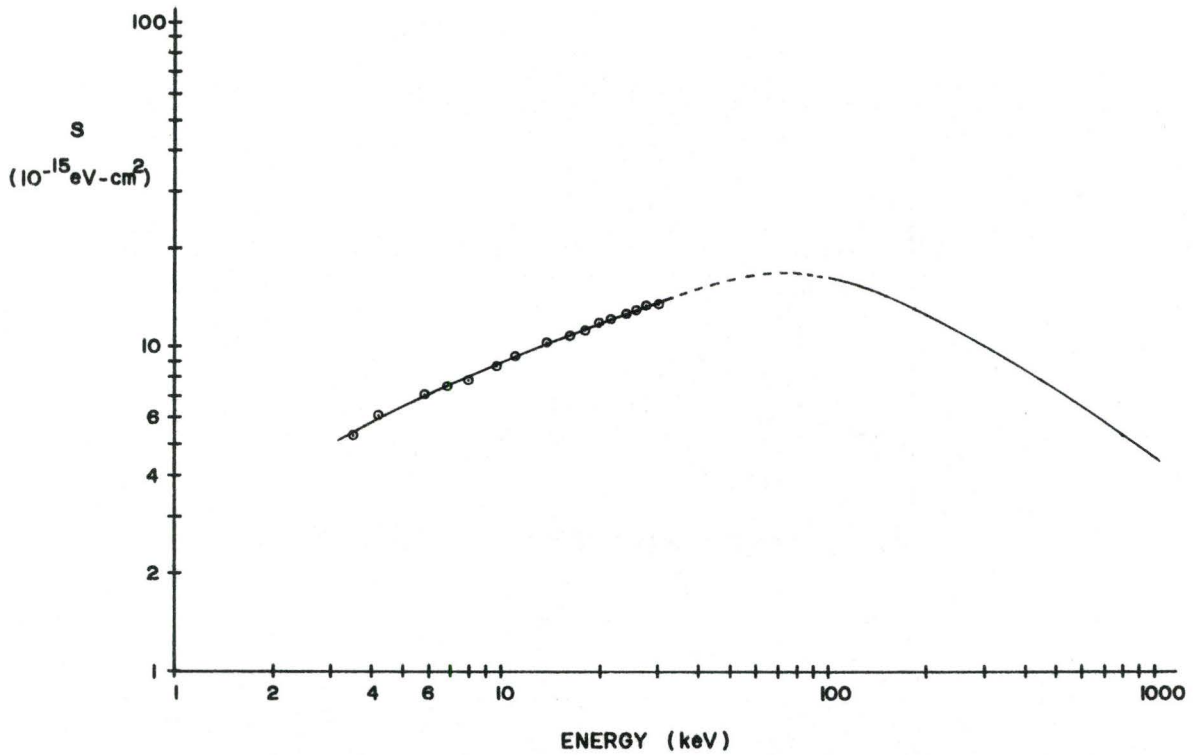
Figure 8 - Matching the Observed S - versus - E Results
in the Energy Region 4<E<30 keV to Those Given by Whaling
(1958) for E>100 keV. The Curves Relate to H[1] Moving in
Carbon.
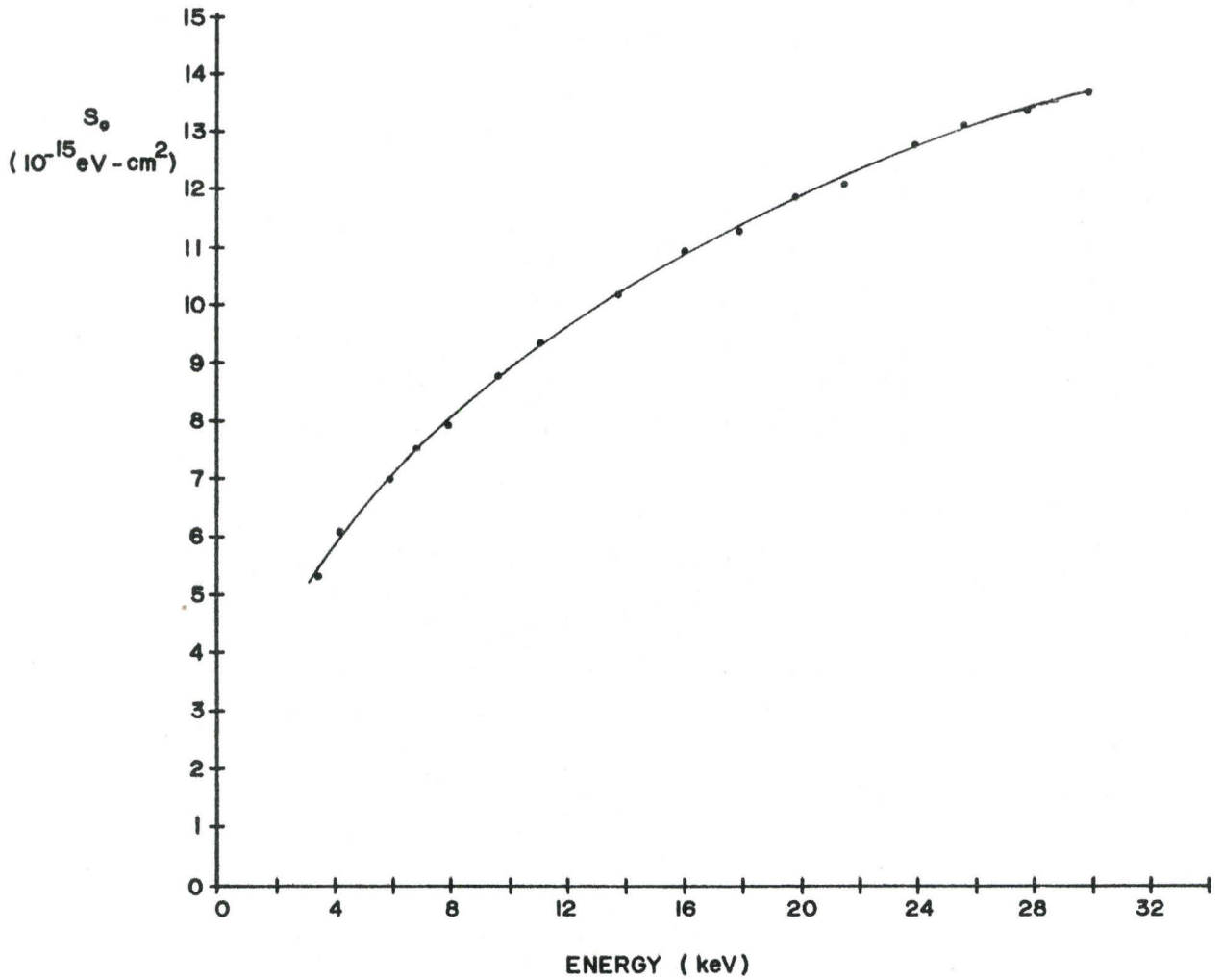
Figure 9 - Plot of Observed Stopping Cross Section, S_o, per Atom as Function of Energy for Case of H^1 Moving in Carbon.

atom-versus-energy curve shown in Figure 9. In the energy interval 4 keV$<$E$<$30 keV this curve is closely described by the empirical equation

$$S_o = 3.5 \times 10^{-14} \ E^{0.41} \ eV-cm^2 \qquad (32)$$

(2) Observations of the Energy Loss of He^4 in Thin Films.

The experiments described in the preceding section were repeated with He^4 as the projectiles and very similar results were obtained. In the energy range 5 keV$<$E$<$30 keV, it was found that the stopping cross-section per atom of aluminum oxide varies with energy according to the following empirical relationship:

$$S_o = 4.6 \times 10^{-15} \ E^{0.44} \ eV-cm^2 \qquad (33)$$

Further, in the energy interval 9 keV$<$E$<$30 keV, the stopping cross-section per atom of carbon is closely described by the empirical relationship

$$S_o = 4.0 \times 10^{-15} \ E^{0.40} \ eV-cm^2 \qquad (34)$$

(3) Experiments with Molecular Ions

Some experiments were carried out with H_2^+, HO^+, H_2O^+, and N_2^+ ions as projectiles. It was found that the results on the energy loss were consistent with the theory that the entire molecule breaks up, on impact, into its constituents, each penetrating the foil with initial velocity equal to the velocity of the impinging molecule.

(4) <u>Some Observations Relating to Charge-Exchange</u>
     <u>Phenomena.</u>

It is well known that a particle, in passing
through a material medium, changes its charge many times.
It is not surprising, therefore, that many of the
particles in our experiments emerged from the film with
a charge that was different from that of the ions imping-
ing upon the film. For example, when O^{++} or O^{+} ions were
used as projectiles, O^{++}, O^{+} and O^{-} ions were detected
in the emerging beam. Neutral oxygen atoms were undoubt-
edly also present, but escaped detection by the electro-
static analyser.

Likewise, with protons incident upon the film,
$\left(H^1\right)^{+}$ and $\left(H^1\right)^{-}$ were both observed in the transmitted beam.
The ratio $\left(H^1\right)^{+}/(H^1)^{-}$ increased rapidly with the energy
of the emerging particles. For example, with a VYNS film,
this ratio was ~ 3 for an emerging energy of 5 keV, ~ 11
for 10 keV, and ~ 30 for 30 keV. On the other hand, when
$\left(He^4\right)^{+}$ was used as the projectile, the ratio $\left(He^4\right)^{+}/(He^4)^{-}$
did not vary rapidly with emerging energy, but had the
approximate value 500 in the energy range 10 keV-30 keV.

The most significant observation for our purpose,
however, was that, within experimental error, the energy
distribution in the beam emerging from a film, and the
most probable value of its energy loss (ΔE_0), are, for a
given atomic projectile, independent of the charge carried
by the atom as it enters and leaves the film. This charge

independence is believed to imply that our observed
stopping cross-sections are weighted averages that
take into account the various possible charge states
that the moving particle may assume during its passage.
It is for this reason that, in this thesis, we have
consistently designated the moving atom as H^1 or He^4,
rather than $(H^1)^+$, $(He^4)^+$, et cetera, in order to
indicate that within the stopping material, the charge
state of the projectile is dependent upon its nuclear
charge, its velocity and the nature of the stopping
medium, but is independent of the charge with which it
enters. Presumably, there is a transition period
during which the entering ion comes to terms with the
stopping material, but in our experiments this period
must have been very brief indeed.

C H A P T E R   I V

Energy Spread in the Beam Transmitted by Thin Films

(1)   The Shape of the Energy Distribution Curves

The reader will have noted in Figure 5 that the
energy distribution amongst the H^1 particles emerging
from Al_2O_3 films is bell-shaped and practically
symmetric. This was true of the other films as well,
and also when He^4 was used as the projectile.

On the other hand, when much heavier projectiles
of the same energy are used, the energy distribution
among the particles emerging from the film is markedly
assymmetric. Figure 10 shows the distribution curve
for A^{40} particles which have passed through the 205Å
aluminum oxide film. These particles entered the film
with an energy of 62.5 keV. The shape of the observed
energy distribution curves for A^{40} was practically
independent in the energy range 10 keV$<$ E $<$ 70 keV
investigated.

The tail of the distribution suggests that an
appreciable portion of the energy lost by A^{40} particles
is being taken up by recoiling atoms, as one would
expect (Harvey, 1960) for a low-speed heavy particle
such as here. When appreciable energy is lost in
such an atomic collision, the particle suffers a
relatively wide angle scattering. For this particle to

reappear in the forward direction, and be observed
in this experiment, it must experience additional wide
angle scattering. Calculations by J.H. Ormrod (1962)
indicate that multiple wide angle scattering in which
a heavy particle emerges from the film in the forward
direction is a frequent enough occurrence to account
for the tail in Figure 10.

In short, we conclude that the presence of a
tail at the low energy end of the energy distribution,
as in Figure 10, is evidence that atomic collisions
are taking place. Conversely, the absence of such a
tail, as was observed for H^1 and He^4 in the 5 keV$<$E$<$
30 keV energy range, is regarded as evidence that the
projectile loses its energy primarily to the electrons
of the stopping medium and, consequently, suffers little
deflection. Certain observations on the angular dis-
tribution of the emerging beam, to be described in the
next chapter, also substantiate this conclusion.

(2)   The Width of the Energy Distribution

(a)   Introduction

In the following, we shall refer to the full
width of the observed energy distribution curves at
half height by W_o. This width is larger than the
corresponding "true width", W. This is due to the
following effect. When the electrostatic analyser is
set to detect particles of a certain energy, it will
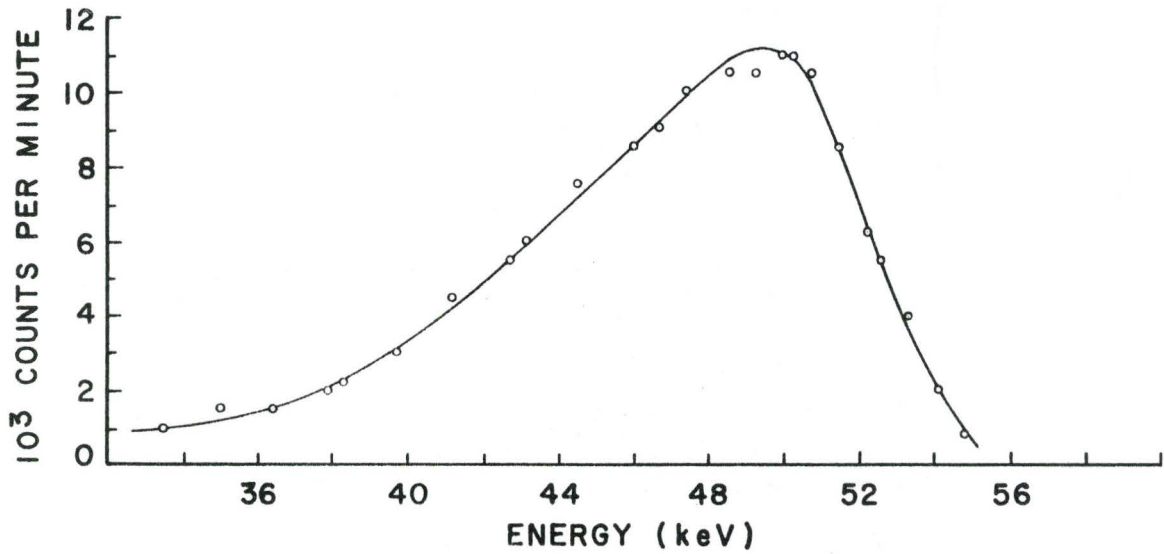
Figure 10 - Energy Distribution Amongst A^{40} Particles after Traversing an Al_2O_3 Film of 205A° Thickness

actually detect particles over a small energy inter-
val, because of its finite resolution. It is for
this reason that we observed (see Figure 5) that the
energy distribution of the beam without a film in its
path had a finite width. We shall denote the full
width of these energy distribution curves by w. Experi-
mentally, it was observed that

$$w = \frac{E}{120} \tag{34a}$$

gives a rough approximation for the magnitude of w.
In this expression w and E should both be expressed
in the same units; for example in keV.

When the actual energy distribution amongst the
particles leaving the film is Gaussian and the energy
distribution of the beam, without a film in its path,
as observed by the electrostatic analyser, is also
Gaussian, then it may easily be shown that the actual
full width, W, is given by

$$W = \sqrt{W_0^2 - w^2} \tag{34b}$$

Here w may be estimated from Equation (34a). For
the purpose of correcting our observed values of W_0
we shall assume Gaussian distribution curves for H^1
and He^4 as projectiles and we shall, therefore, use
Equations (34a) and (34b) to evaluate the actual full
width, W.

Figure 11. Energy Distribution Amongst H[1] Particles, for Various Incident Energies, after Traversing a Carbon Film of 250A° Thickness.

(b) The Straggling in the Energy Loss of H^1 in Carbon

Figure 11 shows about half of the energy distribution curves (so-called straggling curves) that were observed for H^1 particles passing through the 250 Å carbon film. The corresponding energy loss observations in this film have previously been discussed. (III, 1, b). The insets near the top of each curve gives the nominal values of the energy loss, in units of keV, and the observed width, W_o. The values of the average energy $\overline{E}(= E_o - \frac{\Delta E_o}{2})$ can readily be evaluated from these data. They have been tabulated in the first column of Table IV, which has been compiled from the numbers in the insets of Figure 11.

<div align="center">Table IV</div>

$\overline{E}$ keV	W_o keV	W keV	ΔE_o keV	$W/\Delta E_o$
29.9	1.18	1.15	3.86	.30
25.6	1.05	1.03	3.69	.28
21.5	1.00	.98	3.40	.29
17.9	.89	.88	3.19	.28
13.7	.75	.74	2.87	.26
9.6	.63	.62	2.48	.25
6.8	.57	.57	2.12	.27
4.2	.33	.33	1.72	.19

From the Table, it appears that the value of the quotient formed by the corrected width, W, (shown in the third column) and ΔE_0 (shown in the next column) is almost independent of energy in the range $7 < E < 30$ keV, even although W and ΔE_0 are both markedly dependent upon energy. This, of course, means that the energy dependence of W and ΔE_0 are similar. The average value of the quotient, taking also into account the values of W for other observed straggling curves, not shown in Figure 11, is

$$(W/\Delta E_0)_{ave} = .26$$

(c) The Straggling in the Energy Loss of He^4 in Carbon

Figure 12, which is similar to Figure 11, shows some of the straggling curves that were observed when He^4 traversed the carbon film. Table V, which is similar to Table IV, has been compiled from the numbers in the insets of Figure 12 and also from the observed energy distribution curves not shown in this Figure. From this Table we find that the average value of the quotient $W/\Delta E_0$ is

$$\left(\frac{W}{\Delta E_0}\right)_{ave} = .29$$

Again, as for H^1 (see Table IV), we observe that large deviations from this average value occur. However, these deviations appear to be random. This justifies our conclusion that, within experimental error, $W/\Delta E_0$
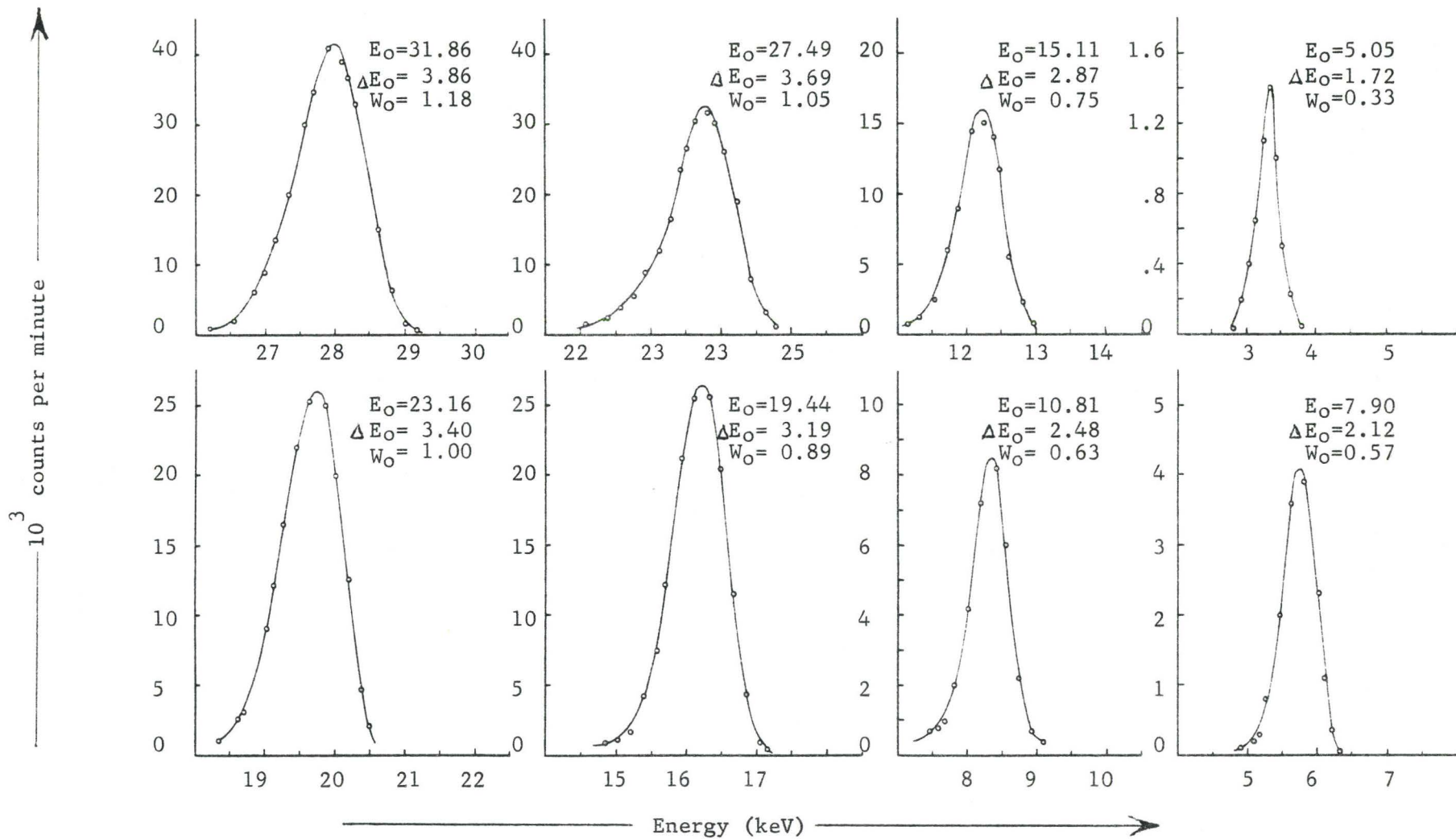
Figure 12. Energy Distribution Amongst He^4 Particles, for Various Incident Energies, after Traversing a Carbon Film of 250° Thickness.
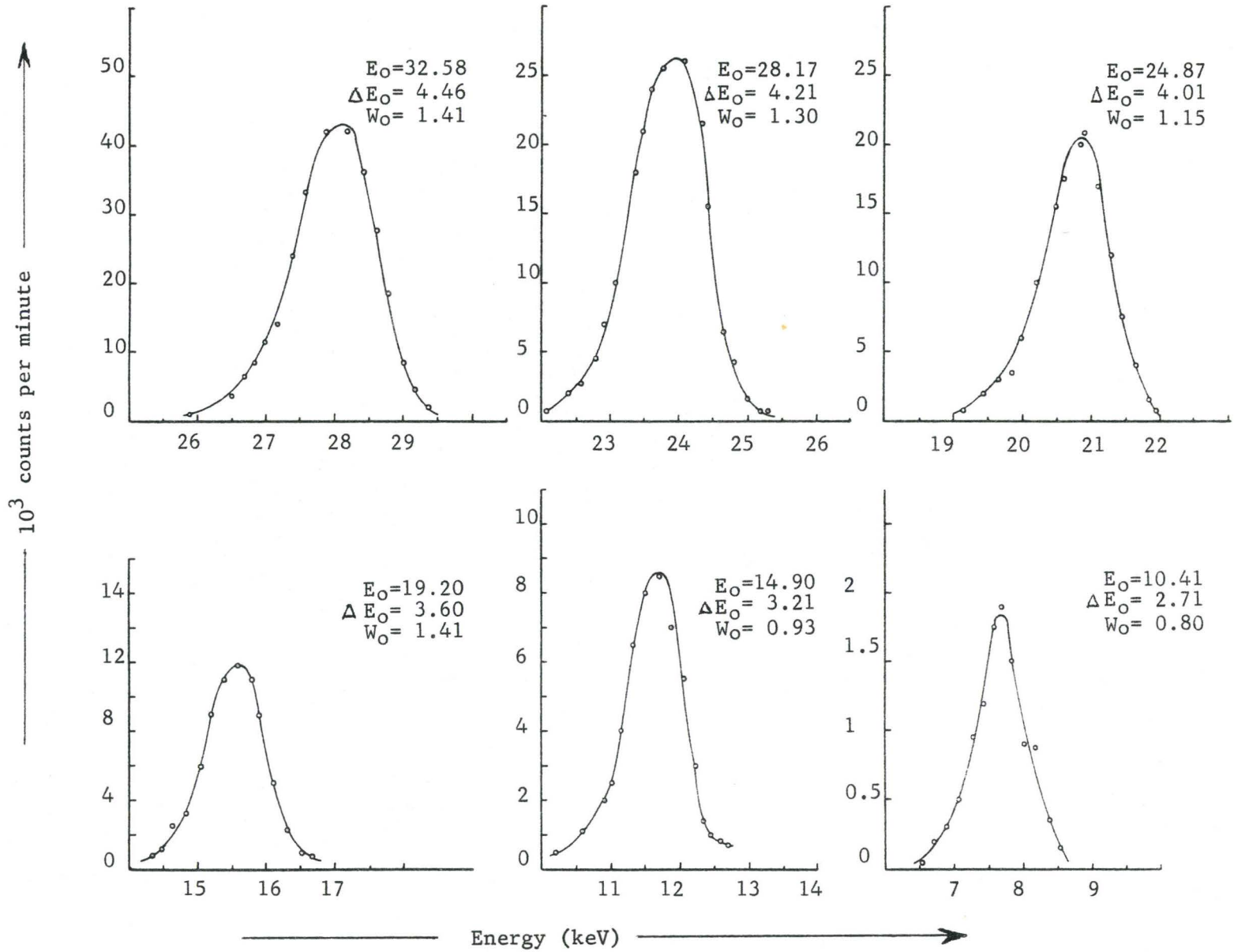
is constant for He^4 in carbon in the energy range studied.

<div align="center">Table V</div>

$\bar{E}$ keV	W_0 keV	W keV	ΔE_0 keV	$W/\Delta E_0$
30.4	1.41	1.39	4.46	.31
28.2	1.39	1.37	4.36	.31
26.1	1.30	1.28	4.21	.30
24.2	1.25	1.23	4.09	.30
22.9	1.15	1.13	4.01	.28
20.0	1.15	1.14	3.75	.30
17.4	1.08	1.07	3.60	.30
15.2	.92	.91	3.38	.27
13.3	.93	.92	3.21	.29
11.5	.88	.87	3.04	.29
9.1	.80	.79	2.71	.29

(d)   The Straggling in the Energy Loss of H^1 in Al_2O_3

In Table VI, which is similar to Table IV, we have tabulated some typical observations obtained with the 205Å aluminum oxide foil for the $\theta = 2.5^o$ film. The corresponding energy loss observations of H^1 in the $\theta = 2.5^o$ film have previously been discussed (III, 1, a). The average value of $W/\Delta E_0$ for the $\theta = 2.5^o$ film is

$$(W/\Delta E_0)_{ave} = .36$$

Table VI

$\overline{E}$(keV)	W_O(keV)	W(kev)	ΔE_O(keV)	$W/\Delta E_O$
$t' = 205\overset{\circ}{A}$		$(\theta = 2.5^{\circ})$		
31	1.30	1.27	3.4	.37
27	1.19	1.17	3.2	.37
23	1.12	1.10	2.9	.38
16	1.00	.99	2.6	.38
12	.85	.84	2.25	.37
8	.65	.64	1.95	.33
6	.50	.50	1.62	.31
4	.45	.45	1.30	.35

Roughly the same value of $W/\Delta E_O$ was also observed for the $\theta = 42.5^{\circ}$ ($t' = 278\overset{\circ}{A}$), the $\theta = 57.5^{\circ}$ ($t' = 383\overset{\circ}{A}$) and the $\theta = 67.5^{\circ}$ ($t' = 536\overset{\circ}{A}$) films. However, we shall see later [Equation (49)] that $W/\Delta E_O$ should depend upon film thickness in the following manner:

$$\frac{W}{\Delta E_O} \propto \frac{1}{\sqrt{t'}}$$

This means that $W/\Delta E_O$ should decrease as t' increases. This dependence was not observed and, unfortunately, we must conclude that our observed energy distributions for the larger angles θ are too wide. The reason for this discrepancy is thought to be due to the following effect.

Our Al_2O_3 films were not perfectly flat but possessed small ripples. The area of these

irregularities was of the order of the cross-sectional
area of the bombarding ion beam. When such a film is
normal to the incident ion beam, practically all par-
ticles traverse nearly the same film thickness. When
the film is rotated through a certain angle θ_O, the
average film thickness, as seen by the ion beam, is
approximately given by

$$\overline{t'} = \frac{t}{\cos \theta_O}$$

However, owing to small ripples, variations in θ,
around the average value θ_O, will occur. Thus some
particles will traverse more film material and others
will traverse less film thickness than the average
value $\overline{t'}$. This effect will noticeably broaden the
width, W_O, only when θ is appreciably larger than zero.
The small ripples, however, will only slightly effect
the observed energy loss, ΔE_O. Thus, although we con-
clude that our observed widths, W_O, for the energy dis-
tribution curves corresponding to the larger angles θ
are wrong, we still believe that the corresponding
observed ΔE_O values are approximately correct.

(e) The Straggling in Energy Loss of He^4 in
Al_2O_3

No detailed experiments in which θ was varied
were carried out with He^4 in passing through Al_2O_3
films. In Table VII, which is similar to Table VI,

most of the observations pertaining to the energy loss
measurements of He^4 in passing through the 205Å film
have been tabulated.

Table VII

$t' = 205$Å $(\theta = 2.5°)$				
$\overline{E}$(keV)	W_o(keV)	W(keV)	ΔE_o(keV)	$W/\Delta E_o$
30	1.61	1.59	4.2	.38
26	1.34	1.32	4.0	.33
24	1.40	1.39	3.8	.37
21	1.12	1.10	3.6	.31
19	1.24	1.23	3.4	.36
16	1.10	1.09	3.3	.33
14	1.05	1.04	3.0	.35
11	1.08	1.08	2.8	.39
9	.90	.90	2.5	.36
7	.78	.78	2.3	.34

The average value of $\Delta E_o/W$, as obtained from Table VII
is $\Delta E_o/W = .35$.

(f) Summary of Results

Table VIII summarizes the observed results for
the full widths of the energy distribution curves for
H^1 and He^4 in passing through a 205Å Al_2O_3 film and
a 250Å carbon film respectively. The straggling data
from this Table will be discussed in Chapter VI.

Table VIII

Film	$W/\Delta E_o$	
	for H^1	for He^4
205Å Al_2O_3 Film	$.36 \pm 0.02$	$.35 \pm 0.02$
250Å Carbon Film	$.26 \pm 0.02$	$.29 \pm 0.01$

C H A P T E R   V

Observations On the Angular Distribution of the Beam
Emerging From Thin Films

For this experiment, the apparatus was modified
in the manner shown in Figure 4. Ideally, both S_3 and
S_5 should have been circular apertures, or S_3 should
have been an infinitely long narrow slit and S_5 a
narrow slit of finite length. In the first case, one
obtains easily interpretable results and in the latter
case one observes "true" angular distribution curves
directly. In practice, however, S_3 and S_5 were narrow
slits whose long dimensions (0.125" for S_3 and 0.5" for
S_5) were perpendicular to the plane of the paper and
were, of course, finite. Consequently, in every position,
ϕ, the detector accepted particles that had suffered
net deflections over a complicated range of angles.
The results of this crude experiment, however, were
adequate for our purpose .. which was to confirm our
suspicion that the H^1 and He^4 particles under study
suffered relatively few wide angle deflections; that is,
relatively few atomic collisions. The film used in
this experiment was a VYNS film, in which ΔE_0 was about
one-third of its value for the $205\overset{O}{A}$ aluminum oxide foil.

Figure 13, which is a plot of the output of the
electron multiplier as a function of its angular position,
shows results obtained with H^1, He^4 and A^{40}, each at two
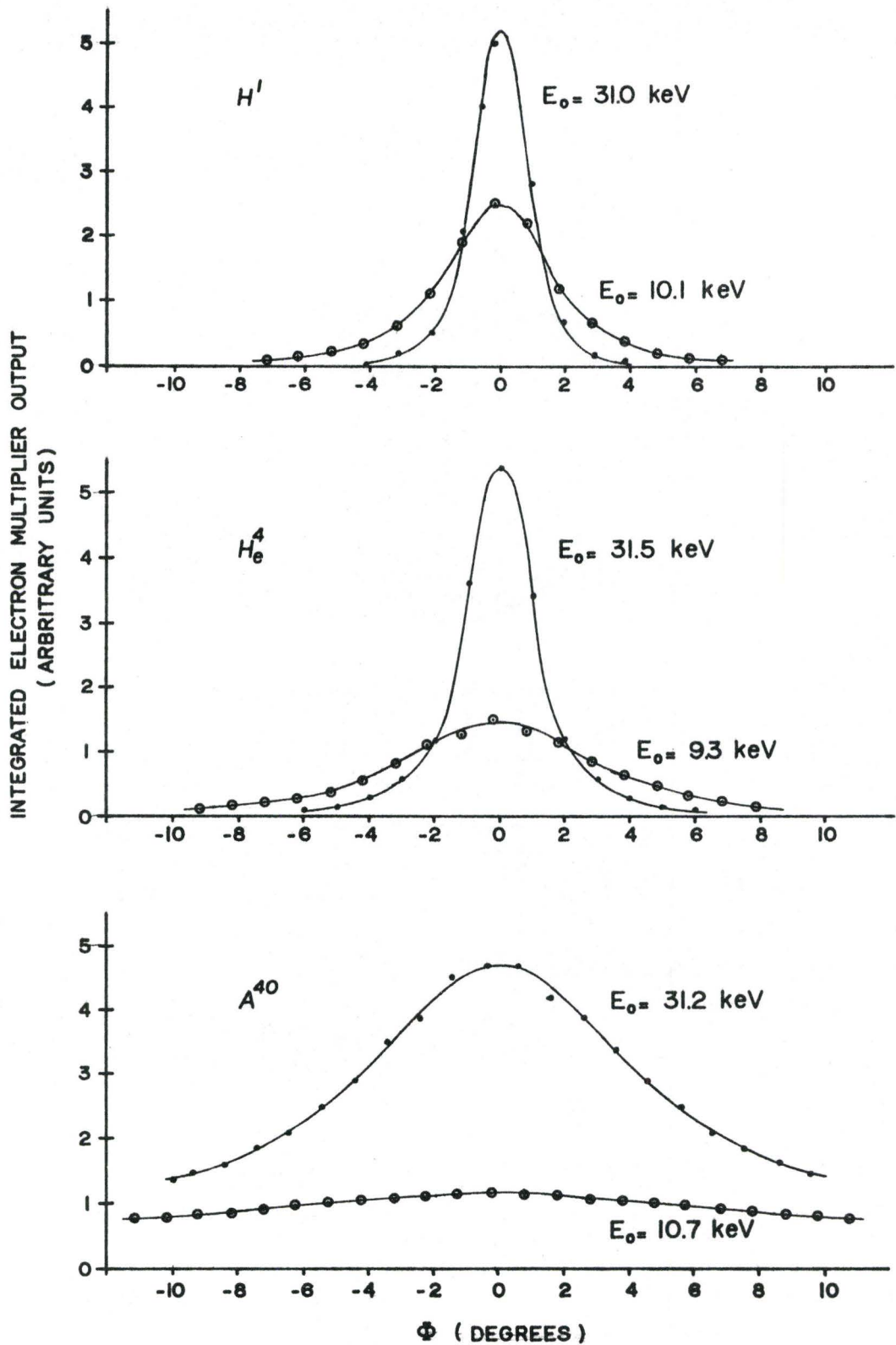
FIGURE 13 - Angular Distribution Amongst H^1, He^4 and A^{40}
Particles after Emerging from a VYNS Film.

different values of incident energy. For a given pro-jectile, the incident current was the same for the two curves. Evidently the A^{40} particles have suffered wide-angle deflections, whilst the deflections suffered by H^1 and to a somewhat lesser extent, He^4, are primarily small-angle ones, especially at the higher value of the energy. It is a simple problem (VI-1) in mechanics to show that, if H^1 and He^4 were losing an appreciable amount of this energy in elastic collisions (with atoms of the stopping medium), the average scattering angle would be much larger than we have observed. Thus, it follows from this experiment that, in the energy range investigated, H^1 and He^4 lose their energy mainly to electrons in the stopping medium. This conclusion is consistent with the nearly symmetric energy distribution curves discussed in the preceding chapter and suggests that our observed S_o's, which refer to particles moving in the forward direction, are practically identical with S_e, the electronic component of the total stopping cross-section per atom.

The broad angular distribution curves for A^{40} are also consistent with the conclusions of the previous chapter. These curves are indicative of atomic colli-sions, as were the pronounced low-energy tails that characterize the energy distributions for this heavy particle.

C H A P T E R   V I

Interpretation of Results

(1) Calculation of the Energy Lost in Atomic Recoils for H^1.

In the following, a calculation will be made which will allow us to use our angular distribution data to make a quantitative estimate of the energy lost in atomic recoils. We shall find that, at energies greater than a few keV, only a small fraction of the total energy lost by H^1 is lost in this way.

The maximum energy transfer, T_{max}, of a particle of mass M_1 and a kinetic energy E in a head-on collision with a target particle of mass M_2 at rest equals

$$T_{max} = \frac{4 M_1 M_2}{(M_1 + M_2)^2} E \tag{35}$$

In a glancing collision, where the particles are deflected through a relative deflection angle α, the energy transfer, T, equals

$$T = T_{max} \sin^2 \frac{\alpha}{2} \tag{36}$$

The relation between the deflection angle, ϕ, of the projectile in the laboratory co-ordinates and the relative deflection angle is

$$\tan \phi = \frac{M_2 \sin \alpha}{M_1 + M_2 \cos \alpha} \tag{19}$$

For H^1 travelling in VYNS ($C_4H_5O_2Cl$)

$$M_1 \leq M_2$$

Hence, it may easily be shown that

$$\frac{\alpha}{2} \leq \phi < \alpha \tag{37}$$

Suppose the square of the resultant scattering angle, Φ, (in laboratory co-ordinates), after passing through a sheet of matter is small (as was the case for our measurements of H^1 above a few keV). Then essentially all the individual scattering angles, ϕ_i, (and consequently α_i) will also be small. Therefore (Bohr - 1948 - Equation 2.5.1)

$$\overline{\Phi^2} = \sum_i \phi_i^2 \tag{38}$$

where the summation extends over all scattering events in the process of traversal of the film.

The energy loss in a single scattering event for a small deflection angle, α_i, is given approximately by [see Equation (36)]

$$T_i = T_{max} \left(\frac{\alpha_i}{2}\right)^2$$

The total energy loss, ΔE_n, of the particles corresponding to the resultant scattering angle $\sqrt{\overline{\Phi^2}}$ is

$$\Delta E_n = \sum_i T_i = \sum_i T_{max} \left(\frac{\alpha_i}{2}\right)^2$$

The subscript, n, in this formula and others to follow, denotes that only the loss in atomic recoils has

been considered.

If the film is _thin_ (as in our angular distribution experiments) the energy of the particle is approximately constant, in which case T_{max} is seen to be approximately constant [Equation (35)]. Then the preceding equation may be re-written

$$\Delta E_n = T_{max} \sum_i \left(\frac{\alpha_i}{2}\right)^2$$

By utilizing Equation (37) we see that

$$\Delta E_n < T_{max} \sum_i \phi_i^2$$

Upon substitution of Equations (35) and (38), this expression becomes

$$\Delta E_n < \frac{4 M_1 M_2}{(M_1 + M_2)^2} E \overline{\phi^2} \qquad (39)$$

from which an upper limit to the energy lost in atomic collisions may be calculated, provided the angular distribution is known. This we shall now do.

The most probable energy loss, ΔE_o, of H^1 in traversing the VYNS film, which was employed in our angular distribution experiments, was

$$\Delta E_o \simeq 0.6 \text{ keV at } \bar{E} \simeq 10 \text{ keV}$$

and

$$\Delta E_o \simeq 0.3 \text{ keV at } \bar{E} \simeq 4 \text{ keV} \qquad (40)$$

The root mean square of a Gaussian distribution curve is equal to its _half_-width. Our angular distribution curves are approximately Gaussian. They are sharper, however, than the true angular distribution curves

because slit S_3 (see Figure 4 and also Chapter V) had a finite rather than an infinite length. On the other hand, the half widths of the experimental curves are significantly broadened (by about 0.5 degrees) because of the finite acceptance angle of the detector. Taking these factors into account, it appears that no serious error is introduced by assuming that $\sqrt{\overline{\phi^2}}$ is equal to the half width of our observed angular distribution curves.

The half width of the distribution curve for, say, E_0 ($\simeq \bar{E} = E_0 - \dfrac{\Delta E_0}{2}$) = 10 keV in Figure 13 is about 2 degrees. Thus

$$\sqrt{\overline{\phi^2}} = 2^0 = 2 \times \frac{2\pi}{360} \text{ radians.}$$

Hence

$$\overline{\phi^2} = \left(\frac{2 \times 2\pi}{360}\right)^2 \tag{41}$$

For VYNS ($C_4H_5O_2Cl$), M_2 in Equation (39) can have different values. The average value is $\sim$10 amu. Substituting this value and $M_1 = 1$ amu for H^1, together with Equation (41) into Equation (39) we find for E = 10 keV

$$\Delta E_n < 0.004 \text{ keV}$$

Hence, compared to the total observed energy loss, [Equation (40)] of 0.6 keV (at $E \simeq 10$ keV) it is indeed true that

$$\Delta E_n << \Delta E_0$$

This means that atomic collisions cannot account for the energy loss, ΔE_0. Therefore, atomic hydrogen at E =

10 keV loses its energy mainly to the electrons of the stopping medium.

Similarly, at $E = 4$ keV, we find, by means of our observed angular distribution curves for H^1 at lower energies, which have not been shown in Figure 13, that

$$\Delta E_n < 0.064 \text{ keV}$$

The total energy loss, ΔE_0, at this energy, however, equals (Equation 40)

$$\Delta E_0 \simeq 0.3 \text{ keV}$$

Hence, we conclude that H^1 with a kinetic energy above* a few keV loses its energy mainly to the electrons of the stopping medium.

At this point, a remark might be made concerning the energy loss of He^4. Previously, we concluded that, for energies greater than a few keV, both He^4 and H^1 lose their energy mainly to electrons, although, as we shall see in the next section, the theory does predict a small but finite loss of energy in atomic recoils for both of these atomic projectiles. The relative importance of this mechanism of energy loss is predicted to be appreciably larger (roughly five times) for He^4 than for H^1. The observed angular distribution curves of the transmitted beam are in qualitative agreement with the prediction, inasmuch as the relative widths of the

---

* At higher energies, above ~ 100 keV, protons lose energy by Coulomb excitation and ionization of the electrons in the stopping medium.

observed angular distribution curves of the trans-
mitted beam are larger for He^4 than for H^1.

(2)   Comparison of Observed Cross-section, S_o, with Theory

On the basis of the energy distributions in the
transmitted beams of H^1 and He^4, we concluded that these
particles lose their energy primarily to the electrons
of the stopping medium rather than in atomic collisions.
The results of the angular distribution experiments are
in agreement with this conclusion. We should further
note that the predictions of the theory are also in
accord with this conclusion. In order to show this,
we have plotted in Figure 14 (a) the S_e- versus - E
curve [using Equation (1)]; (b) the S_n- versus - E curve
[using Equation (10)], and (c) the experimentally observed
S_o- versus - E curve, in each case for H^1 passing through
carbon. Figure 15 shows the corresponding curves for
He^4 passing through carbon. Figures 16 and 17, respec-
tively, show these corresponding curves for H^1 and He^4
passing through Al_2O_3. The S_e and the S_n curves for the
slowing down process in Al_2O_3 were obtained by taking
as average values $Z_2 = 10$ and $M_2 = 20$.

In these figures, the calculated values of S_n are
much less than those of S_e, although the difference is
not as marked for He^4 as for H^1. Moreover, in our
experiments, only a small portion of S_n comes into the
picture, inasmuch as most of the atoms that suffer appreci-

Figure 14 - Composite Plot Showing (a) Calculated Nuclear
Component of Total Stopping Cross Section per Atom, (b)
Calculated Electronic Component of Total Stopping Cross
Section per Atom, and (c) Observed Stopping Cross Section
per Atom, All as a Function of Energy, for H^1 Passing
through Carbon.

Figure 15 - Composite Plot Showing (a) Calculated Nuclear
Component of Total Stopping Cross Section per Atom, (b)
Calculated Electronic Component of Total Stopping Cross
Section per Atom, and (c) Observed Stopping Cross Section
per Atom, All as a Function of Energy, for He^4 Passing
through Carbon.

Figure 16 - Composite Plot Showing (a) Calculated Nuclear Component of Total Stopping Cross Section per Atom, (b) Calculated Electronic Component of Total Stopping Cross Section per Atom, and (c) Observed Stopping Cross Section per Atom, All as a Function of Energy, for H^1 Passing through Al_2O_3
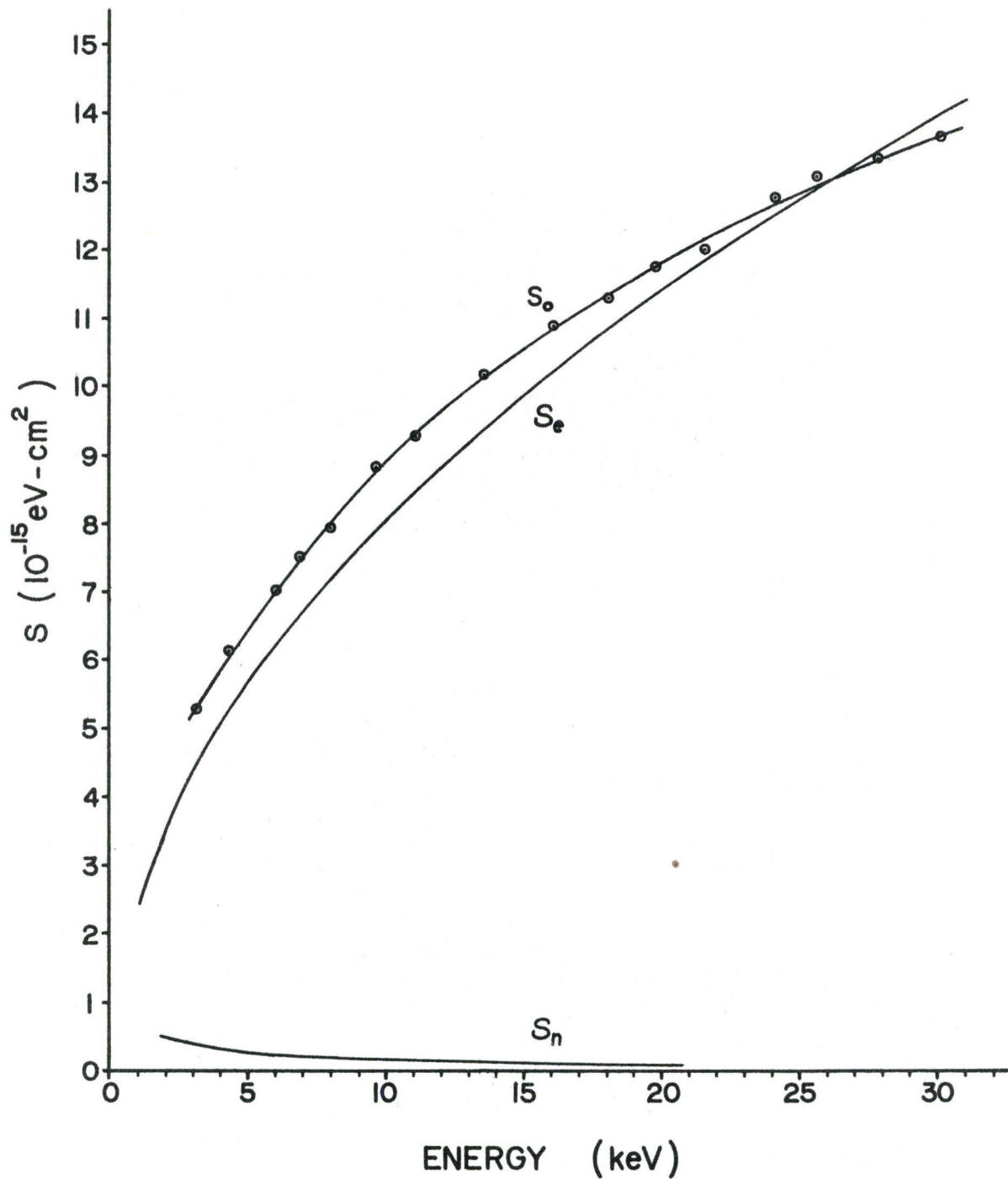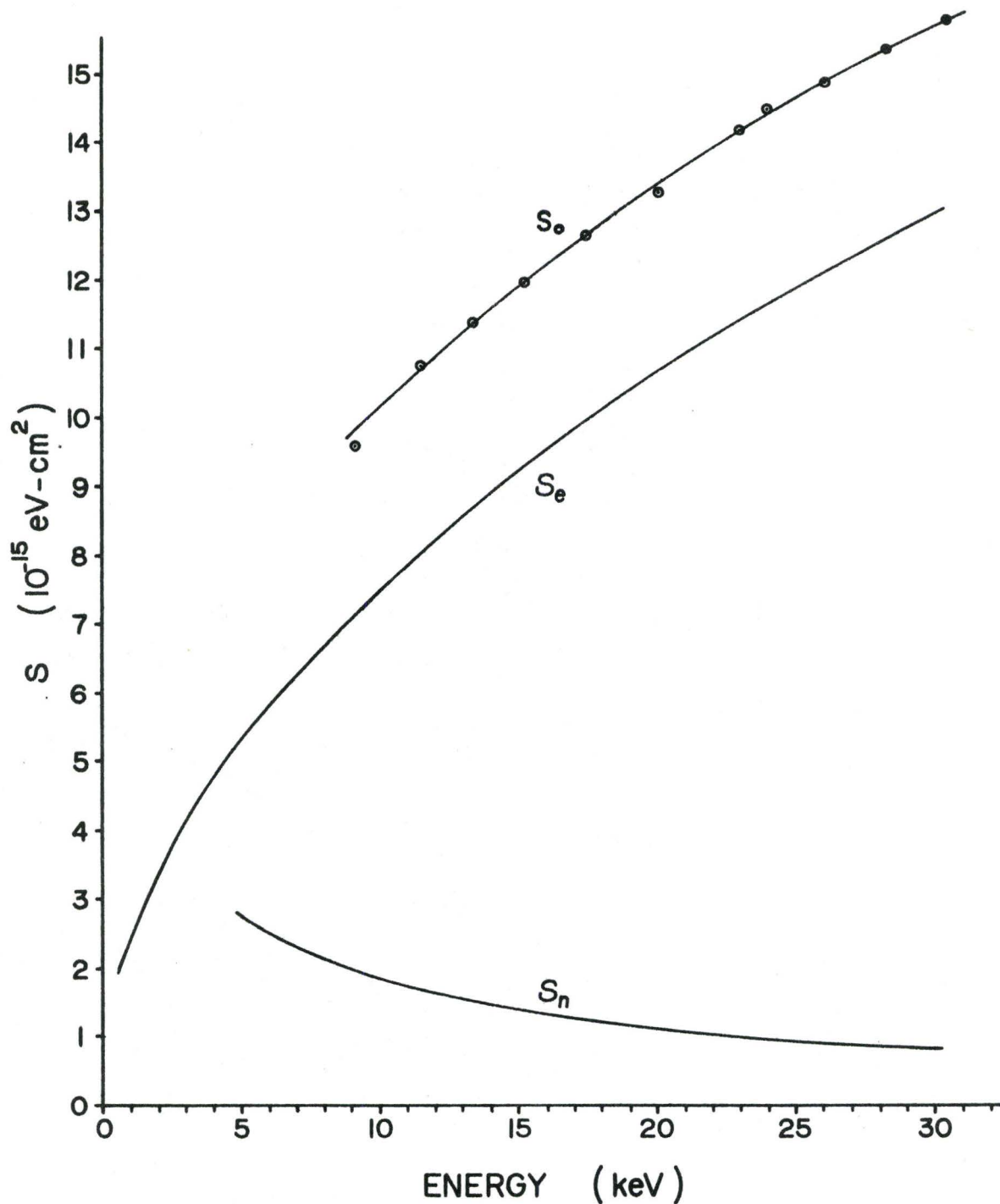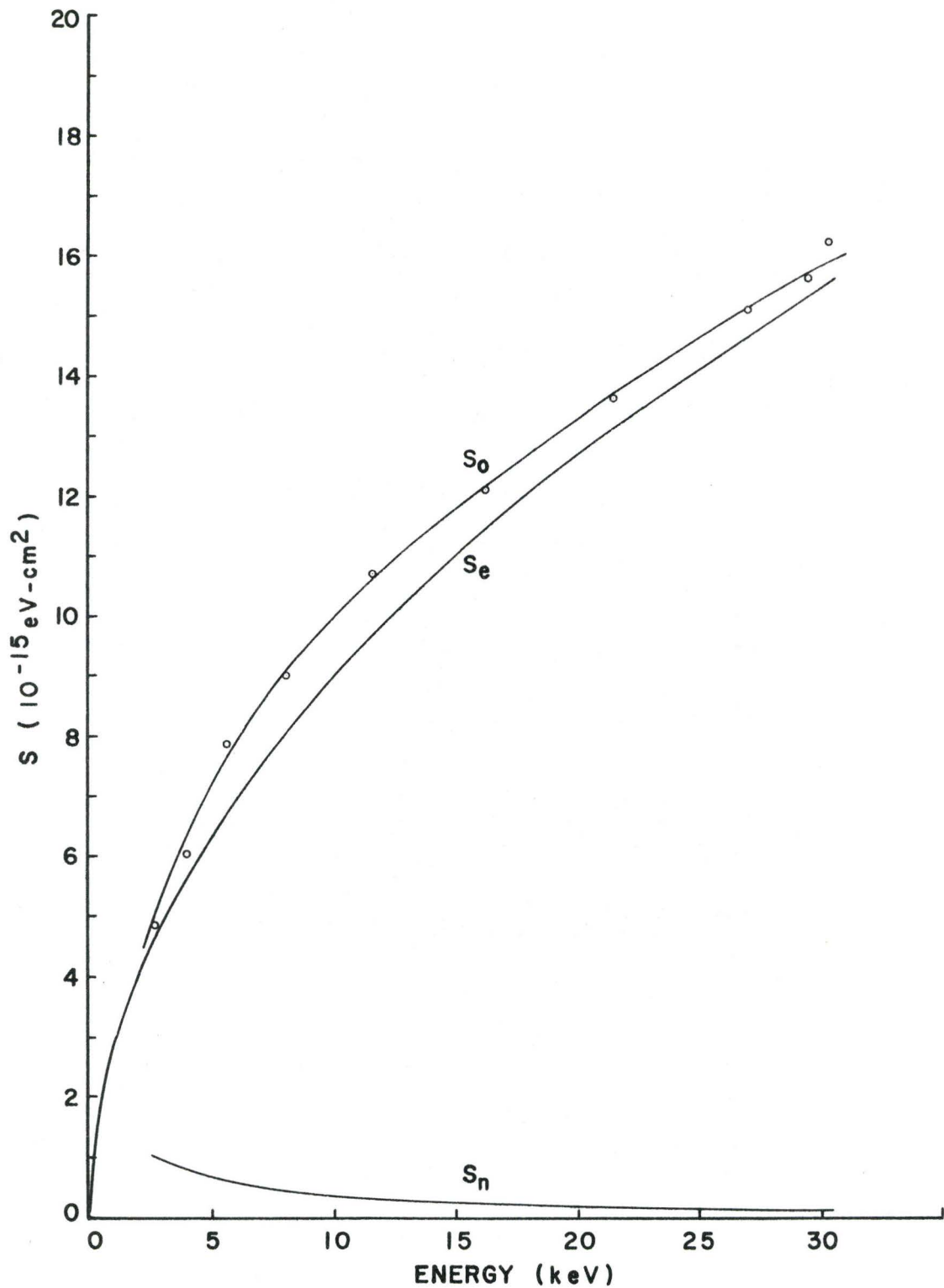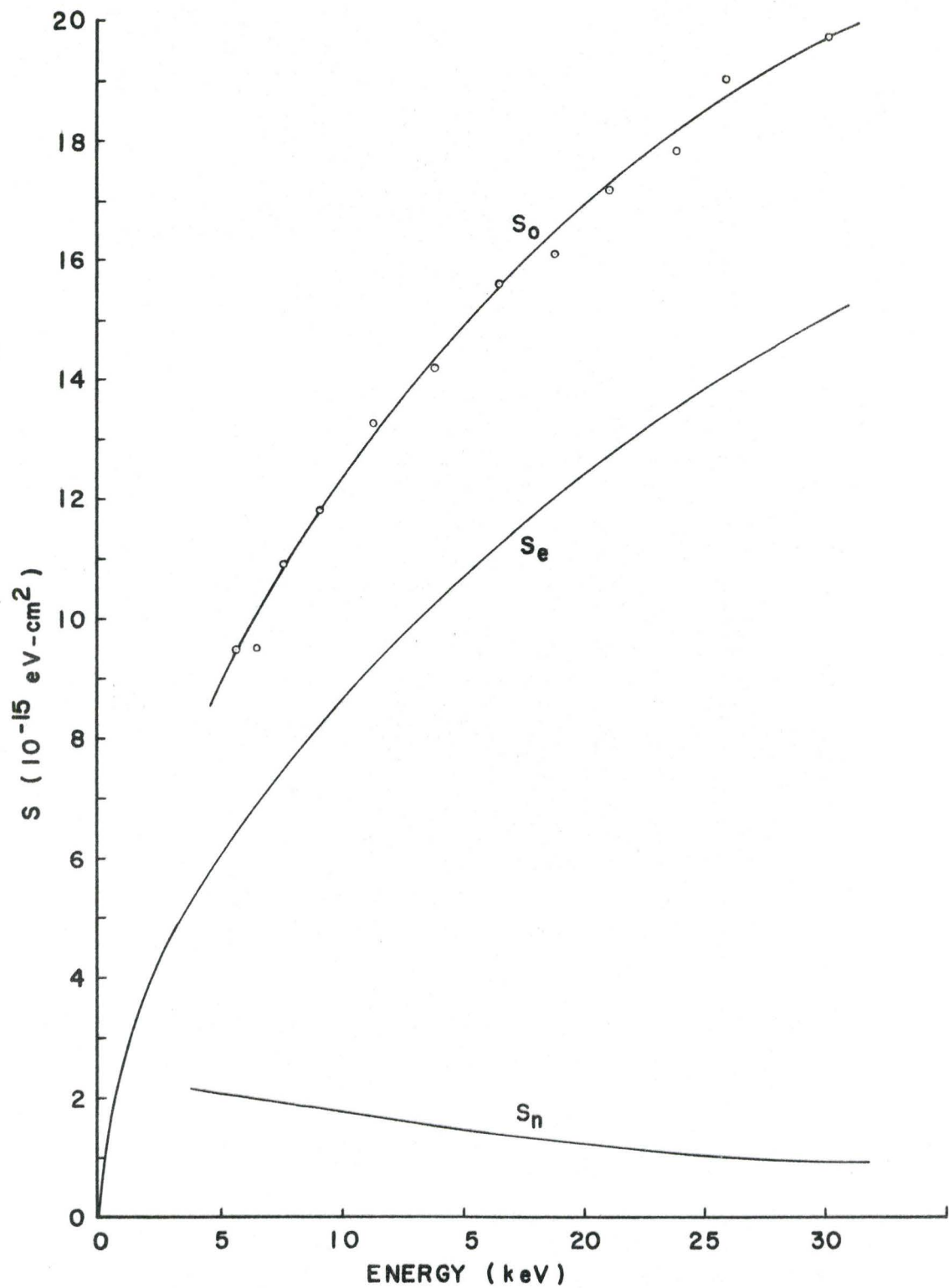
Figure 17 - Composite Plot Showing (a) Calculated Nuclear
Component of Total Stopping Cross Section per Atom, (b)
Calculated Electronic Component of Total Stopping Cross
Section per Atom, and (c) Observed Stopping Cross Section
per Atom, All as a Function of Energy, for He^4 Passing
through Al_2O_3

able energy loss in atomic collisions are scattered out of the beam and consequently, are not observed. The multiple wide-angle scattering event, mentioned earlier for A^{40}, in which the particle regains its original direction, is relatively rare for H^1 and He^4 at the energies used.

Hence, on theoretical, as well as experimental, grounds, we appear justified in identifying our observed S_o with S_e, the electronic component of the total stopping cross-section per atom. With this understanding, let us now compare the form of the S_o-versus-E curve with that predicted for S_e.

We note that the empirical expressions for S_o [Equations (31), (32), (33) and (34)] do not display the same energy dependence that is predicted for S_e, the electronic component of the stopping cross-section per atom. Whereas S_e is predicted to vary as $E^{1/2}$, our observed S_o's vary as $E^{0.45}$ and $E^{0.44}$ for H^1 and He^4 respectively, in Al_2O_3, and as $E^{0.41}$ and $E^{0.40}$ for H^1 and He^4 in carbon, respectively.

Three explanations for the discrepancy suggest themselves:

(a) The electronic component S_e does not correspond closely to our observed S_o's, as we have assumed. Instead, there is a not-insignificant S_n contribution which, since it increases with decreasing energy, causes the S_o-versus-E curve to be flatter than the $S_e \propto \sqrt{E}$

one, as is experimentally observed. This effect, at any given energy, should be much more pronounced for He^4 than for H^1 - a prediction which appears not to be borne out by experiment.

(b) We are operating in a region where electronic losses are the dominating ones all right, but the transition to the $(\ln E)/_E$ region has already begun. This effect, also, would cause the S_o-versus-E curve to be flatter than the $S_e \propto \sqrt{E}$ one. Moreover, the effect should be more noticeable, at any given energy, for H^1 than for He^4, a prediction not borne out by experiment.

(c) The predicted dependence of S_e upon E is somewhat in error. We appear to be left with this alternative.

Finally, let us compare the absolute magnitudes of the observed S_o's and the calculated S_e's. For H^1, as can be seen from Figures 14 and 16, the ratio S_o/S_e is never far from unity over the entire energy range studied. Indeed, the uncertainties in the thicknesses of our film are such that the average value of the ratio may be even closer to unity than appears to be the case in the figures. For He^4, however, (see Figures 15 and 17), the absolute values appear to be systematically in error.

At this point we quote from a recent private communication from Professor Lindhard: "It should be emphasized that Equation (4) is approximate in more

than one sense. The constant $\xi_e \simeq Z_1^{1/6}$ is based

on Thomas-Fermi arguments and it is to be expected that

fluctuations around this constant can occur, especially

for $Z_1 \leq 10$. Moreover, a precise proportionality to

v (i.e. $\sqrt{E}$) will not be correct over the whole of the

velocity region $v < v_1$, $(v_1 = v_o Z_1^{2/3})$." It would appear

that our observations of the energy dependence of S_o,

and of the systematic difference between S_o and S_e

values for He^4, illustrate the relevance of Professor

Lindhard's remarks.

(3) Comparison of $W/\Delta E_o$ with Theory

The energy distribution amongst the particles

leaving the film arises out of two processes:

(a) Not all particles in traversing the film

suffer the same number of collisions; some particles

suffer more, others undergo fewer, collisions than

some average number.

(b) Not all particles that undergo the same

number of collisions suffer the same energy loss per

collision.

Bohr (1948) investigates the straggling in some

detail. He writes the total energy loss, ΔE, of a

particle in traversing a sheet of matter of thickness,

t, as

$$\Delta E = \sum_i T_i n_i \qquad (42)$$

Here n_i is the number of collisions, for the particle under consideration, in which it transfers the energy T_i per collision. n_i will be distributed around its mean value, $\overline{n_i}$, according to a Poisson distribution. Thus

$$P(n_i) = \frac{\overline{n_i}^{n_i} \overline{e}^{\overline{n_i}}}{n_i!} \tag{43}$$

The average value of ΔE, which we have denoted as ΔE_0 is given by

$$\Delta E_0 = \sum_i T_i \overline{n_i} \tag{44}$$

with a mean square deveation.

$$\Omega^2 = \overline{(\Delta E - \Delta E_0)^2} = \sum_i T_i^2 \overline{(n_i - \overline{n_i})^2} = \sum_i T_i^2 \overline{n_i} \tag{45}$$

since $\overline{(n_i - \overline{n_i})^2} = \overline{n_i}$ for a Poisson distribution. Here Ω represents the half width of the energy distribution, amongst the particles leaving the sheet of matter, at half its maximum height. Thus

$$W = 2\Omega \tag{46}$$

Equation (42) is equivalent to

$$\Delta E_0 = Nt \int T d\sigma \tag{47}$$

where $\int T d\sigma = S$ [see Equation (29)] represents the stopping cross-section per atom. Equation (45) is equivalent to

$$\Omega^2 = Nt \int T^2 d\sigma \tag{48}$$

We note from Equations (47) and (48) that

$$\frac{\Omega}{E_0} \propto \frac{1}{\sqrt{t}} \qquad (49)$$

From the foregoing it is evident that the relationship between Ω and ΔE_0 can only be found if the energy transfer, T, can be expressed as a function of the differential cross-section, $d\sigma$. This, of course, involves a knowledge of the mechanism of the energy loss.

In our experiments with H^1 and He^4 as projectiles, the loss in energy to electrons was studied and the results compared with the theory of Lindhard and Scharff (1961). One of these author's Lindhard, has also studied the straggling in the energy loss and finds (Lindhard, 1954, Equation 4.16) for a particle moving in a degenerate Fermi gas that

$$\Omega^2 = 4\pi Z_1^2 e^4 \rho \, L_\Omega t \qquad (50)$$

Here ρ is the electron density. Lindhard has considered the form of L_Ω and finds that _over a wide region of densities_ L_Ω is proportional to $\rho^{-1/2}$. In an actual stopping medium, of course, the electron density will strongly vary as the particle moves a distance of the order of the interatomic distances in the absorber. However, since the form of L_Ω does not depend upon the magnitude of ρ it is meaningful to take for ρ the average electron density in the stopping medium. In the calculations to follow, we shall, therefore, take for ρ the average electron density of the

stopping material.

For low velocities Lindhard obtains the following estimate for a degenerate electron gas

$$\frac{\Omega 2}{\Delta E_o} \simeq (5mv^2 \hbar \omega_o)^{1/2} \tag{51}$$

where

$$\omega_o = \sqrt{\frac{4\pi e^2 \rho}{m}}$$

is the so-called plasma frequency. Here m is the electronic mass. $\Omega/\Delta E_o$ can now be found by substitution of

$$\Delta E_o = NS_e t$$

(see section III, 1, a) where S_e is given by Equation (4). On carrying out the substitution and inserting the known values of the constants we find

$$\frac{\Omega}{\Delta E_o} = 6.14 \times 10^4 \left[\frac{(Z_1^{2/3} + Z_2^{2/3})^{3/2}}{Z_1^{7/6} \cdot Z_2} \cdot \frac{\rho^{1/4}}{Nt} \right]^{1/2}$$

Thus, see Equation (46),

$$\frac{W}{\Delta E_o} = 1.23 \times 10^5 \left[\frac{(Z_1^{2/3} + Z_2^{2/3})^{3/2}}{Z_1^{7/6} \cdot Z_2} \cdot \frac{\rho^{1/4}}{Nt} \right]^{1/2} \tag{52}$$

From Equation (52) we observe that $W/\Delta E_o$ is independent of energy. This is in agreement with observation (Chapter IV).

We shall now compare our observed values of $W/\Delta E_o$

with Equation (52). The electron density   can be estimated as follows. For our carbon film we assumed that

$$N = 1.13 \times 10^{23} \text{ atoms/cm}^3$$

Thus

$$\rho = Z_2 N = 6 \, (1.13 \times 10^{23}) \text{ electrons/cm}^3$$

For our Al_2O_3 film we assumed that

$$N = 1.03 \times 10^{23} \text{ atoms/cm}^3$$

and that the average value of $Z_2 \simeq 10$. Thus

$$\rho = Z_2 N = 10(1.02 \times 10^{23}) \text{ electrons/cm}^3.$$

In Table IX, we have tabulated the calculated values of $W/\Delta E_o$. This Table also presents the corresponding observed values of $W/\Delta E_o$ (see Table VIII).

Table IX

Film	H^1		He^4	
	$W/\Delta E_o$ (Observed)	$W/\Delta E_o$ (Theory)	$W/\Delta E_o$ (Observed)	$W/\Delta E_o$ (Theory)
205Å Al_2O_3 Film	.36 ± 0.02	.31	.35 ± 0.02	.22
250Å Carbon Film	.26 ± 0.02	.27	.29 ± 0.01	.20

From this Table we notice that Equation (52) predicts the right order of magnitude for $W/\Delta E_o$.

(4) Conclusion

Thus we conclude that our measurements are in tolerable agreement with the Lindhard and Scharff theory, for loss in energy to electrons of low speed

atomic particles, in more than one sense:

(a) In the energy range studied H^1 and He^4 lose their energy mainly to electrons.

(b) The theory correctly predicts the magnitude of the observed stopping cross-section, S_O, and predicts fairly accurately its energy dependence.

(c) The theory gives a reasonable estimate for the magnitude of $W/\Delta E_O$ and also correctly predicts that this quotient is independent of energy.

Our results, therefore, confirm that for the purpose of energy loss of low speed atomic particles the electrons in the stopping medium may, to a first approximation, be considered as a degenerate Fermi gas (see Appendix).

A P P E N D I X

The Energy Loss of an Atomic Particle in a Degenerate Electron Gas (Sect. I, 2, b)

At high energies the speed of the moving particle is much larger than that of the orbital electrons in the stopping medium. These electrons may, therefore, to a first approximation be considered as stationary. Using arguments of this type Bloch (1933) showed that

$$ -\frac{dE}{dx} \propto \frac{1}{E} \ln E $$

At low energies, i.e. for velocities below the orbital velocities of the electrons the conventional stopping power formula, applicable to fast heavy particles, no longer represents a useful approximation.

Fermi and Teller (1947) deduced an expression for the energy loss at low speeds, for particles much heavier than the electron, in the following manner. In their theoretical considerations they replaced the stopping medium by a degenerate electron gas, in which the maximum electron speed is approximately equal to the velocity, v_0, of the outer electrons in the atoms comprising the stopping medium. In such a gas the moving particle cannot excite, i.e. cannot collide with all the electrons in the Fermi gas. Owing to the Pauli principle only those electrons whose resulting speed after the collision will be outside the occupied zone of the velocity space of the degenerate

electron gas will be scattered.

In a collision between the projectile and an individual electron the change in speed of the latter will be of the order of $\mathbf{v}$, the speed of the moving particle. Fermi and Teller considered the case when $\mathbf{v} \ll \mathbf{v_o}$. Thus only the electrons near the Fermi level will be scattered. In particular, only the electrons within the range $/v_o - v/$ to v_o participate in such collisions. From an evaluation of the density of the electrons for which collisions are not forbidden by the Pauli principle and from an estimate of the collision cross-section Fermi and Teller estimated the order of magnitude of the energy loss per unit time to be

$$- \frac{dE}{dt} \simeq \frac{m^2 e^4 E}{M_1 \hbar^3}$$

Here m is the mass of the electron, M_1 is the mass of the projectile and $\hbar$ is Planck's constant divided by 2π.

The stopping power, $- \frac{dE}{dx}$, can easily be deduced from the above equation. We find

$$- \frac{dE}{dx} \simeq \frac{m^2 e^4}{\hbar^3} \sqrt{\frac{E}{2M_1}}$$

It will be noted that $- \frac{dE}{dx}$ is proportional to the velocity of the moving particle. This velocity dependence is in agreement with the velocity dependence of the Lindhard and Scharff formula $\left[\text{Equation (3)}\right]$ for the stopping cross-section for loss in energy to electrons.

Their expression is a generalization of the Fermi and Teller result and is applicable to all systems.

R_E_F_E_R_E_N_C_E_S

Billington, D.S. and Crawford, J.H. (1961) Radiation
Damage in Solids (Princeton University Press).

Bloch, F. (1933). Ann. Physik. 16, 285

Bohr, N. (1948). Kgl danske Vidensk. mat.-fys.
Medd. 18, No. 8

Davies, J. A. (1960). Can. J. Chem. 38, 1526

Fermi, E. and Teller, E. (1947). Phys. Rev. 72, 399

Harvey, B. G. (1960). Ann. Rev. Nuclear Sci. 10, 235

Holmes, D. K. and Leibfried, G. (1960). J. Appl.
Phys. 31, 1046

Lindhard, J. (1954). Kgl. danske Vidensk, mat.-fys.
Medd. 28, No. 8

Lindhard, J. and Scharff, M. (1953). Kgl. danske
Vidensk. mat.-fys. Medd. 27, No. 15.

Lindhard, J. and Scharff, M. (1961). Phys. Rev. 124,
128

Nielsen, K. O. (1956) Electromagnetically Enriched
Isotopes and Mass Spectrometry (Academic Press,
New York), p. 73.

Ormrod, J. H. (1962) To be published.

Ormrod, J. H. and Duckworth, H. E. (1962) Physics in
Canada, 18, No. 3, 12.

Phillips, J. A. (1953). Phys. Rev. 90, 532

Powers, D. and Whaling, W. (1962). Phys. Rev.126, 61.

Revell, R. S. M. and Agar, A.W. (1955). Brit. J. Appl.
Phys. 6, 23

References - cont'd

Reynolds, H. K., Dunbar, D.N.F., Wenzel, W.A. and
   Whaling, W. (1953). Phys. Rev. <u>92</u>, 732

Seitz, F. and Koehler, J.S. (1956). <u>Solid-State</u>
   <u>Physics</u>, Vol. 2, p. 305.

Whaling, W. (1958). Handbuch der Physik (Springer-
   Verlag, Berlin), Vol. <u>34</u>, 192